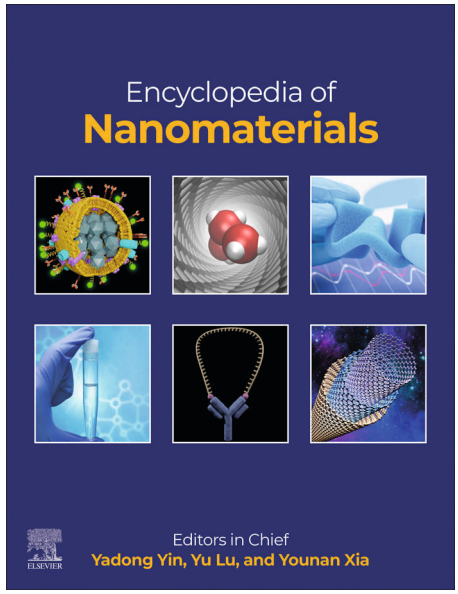

Wang, Hongyu and Zhu, Yong (2023) Mechanical Properties of Nanowires. In: Yadong Yin, Yu Lu and Younan Xia (eds.) *Encyclopedia of Nanomaterials,* vol. 1, pp. 713–729. Oxford: Elsevier.

http://dx.doi.org/10.1016/B978-0-12-822425-0.00079-8

Mechanical Properties of Nanowires

Hongyu Wang and Yong Zhu, Department of Mechanical and Aerospace Engineering, North Carolina State University, Raleigh, NC, United States

Abstract

Mechanical properties of nanowires (NWs) can be different from those of their bulk counterparts, manifesting so-called size effect. Measuring their mechanical properties and understanding their deformation mechanisms are of critical relevance. This article reviews the mechanical properties of three types of NWs – metallic, ionic, and covalent NWs categorized by their bonding types – including Young's modulus, strength, plasticity and fracture. Major mechanical testing methods for NWs such as bending, resonance, and uniaxial tension are also summarized along with key experimental challenges such as sample preparation and effect of boundary conditions. A brief summary and outlook for future research directions are provided.

Graphical Abstract

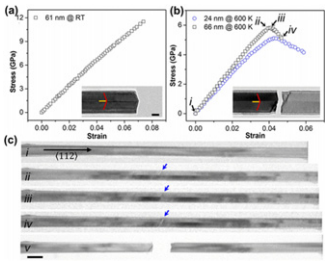

Key Points

- Reviewed mechanical properties of nanowires including Young's modulus, yield strength, plasticity, and fracture.
- Discussed the mechanical properties of nanowires based on their bonding types: metallic, ionic, and covalent bonding.
- Summarized major mechanical testing methods for NWs such as bending, resonance, and uniaxial tension as well as associated experimental challenges.
- Discussed the size effect in mechanical properties of nanowires.

Introduction

As fundamental building blocks of nanotechnology, a wide variety of nanowires (NWs) have emerged in the past few decades (Xia *et al.*, 2003). These NWs exhibit unique and novel mechanical, electrical, magnetic, optical, and catalytic properties. The nanowires are used in a broad range of applications including flexible and stretchable electronics, optoelectronics, energy harvesting and storage and nanoelectromechanical systems (McAlpine *et al.*, 2003; Wang and Song, 2006; Feng *et al.*, 2007; Chan *et al.*, 2008; Takei *et al.*, 2010; Xu *et al.*, 2011; Yao and Zhu, 2015; Yao *et al.*, 2017, 2019; 2018; Zhou *et al.*, 2020). For example, Ag nanowire (NW) networks are widely used as the conductive elements in flexible and stretchable electronics due to their high electric conductivity and mechanical stretchability (Lee *et al.*, 2012; Xu and Zhu, 2012; Yao and Zhu, 2014). The operation and reliability of the NW-based devices call for a thorough understanding of the mechanical properties of NWs that can be quite different from their bulk counterparts. Size and surface effects are dominant for these small-volume materials as their characteristic dimension approaches sub-100 nm. On the other hand, as-synthesized NWs often possess well-defined internal (in contrast to surface) defects such as twinning boundaries (TBs) and stacking faults (SFs). Therefore, such NWs can be ideal model systems to probe how the defects affect the mechanical behaviors of not only NWs but also their bulk counterparts.

In this article, we focus on the mechanical properties of three types of NWs, metallic, ionic, and covalent NWs categorized by their bonding types. We start with the widely used mechanical testing methods for NWs such as bending, resonance, and uniaxial tension using atomic force microscope (AFM), scanning electron microscope (SEM), or transmission electron microscope (TEM), including key experimental challenges such as sample preparation and effect of boundary conditions. Next, the general size effect in mechanical properties at the nanoscale is briefly discussed. Then we summarize the mechanical properties of the three types of NWs measured by nanomechanical testing, including Young's modulus, strength, plasticity and fracture. Finally, we will provide a brief summary and outlook for future research directions in this important area.

Mechanical Testing Methods

Mechanical testing of NWs and 1D nanostructures in general is challenging considering their miniscule size (Zhu *et al.*, 2007; Gianola and Eberl, 2009). The available testing methods can be grouped into two main categories based on the instruments involved, AFM (Li *et al.*, 2010) and electron microscopes including SEM and TEM (Zhu, 2016). Key developments in these two general categories of methods since the 90s are summarized in a recent review (Zhu, 2017). More specifically, the following several methods have been widely used, including resonance in SEM or TEM (Treacy *et al.*, 1996; Poncharal *et al.*, 1999; Chen *et al.*, 2006a), bending using AFM (Wong *et al.*, 1997; Song *et al.*, 2005a; Wu *et al.*, 2005), tension using a nanomanipulation system in SEM (Yu *et al.*, 2000; Zhu *et al.*, 2009), and tension using microelectromechanical systems (MEMS) in either SEM or TEM (Zhu and Espinosa, 2005; Agrawal *et al.*, 2008; Cheng *et al.*, 2014). **Fig. 1**(a)-(d) show the schematics of the four testing methods (Agrawal *et al.*, 2011b) and **Fig. 1**(e) shows the SEM image of a MEMS device for tensile testing of single NWs (Zhu and Espinosa, 2005).

Resonance

Resonance is a simple yet widely used method to measure Young's modulus of NWs. According to a simple beam theory, the resonance frequency of a NW is proportional to the square root of its Young's modulus. Resonance can be excited by thermal (Treacy *et al.*, 1996), electrostatic (Poncharal *et al.*, 1999; Chen *et al.*, 2006a) or mechanical (Dikin *et al.*, 2003; Qin *et al.*, 2012) means. The resonance test has been used to measure Young's modulus of CNTs (Treacy *et al.*, 1996), ZnO (Chen *et al.*, 2006a; Qin *et al.*, 2012), GaN (Nam *et al.*, 2006), Si (Belov *et al.*, 2008), B (Ding *et al.*, 2006), and SiO_2 NWs (Dikin *et al.*, 2003).

AFM Bending

AFM can be operated in four modes for mechanical characterization – (normal) contact mode, lateral force mode, nanoindentation mode, and contact resonance mode (Zhu, 2017). The first two modes are widely used in mechanical testing of NWs, in which a NW specimen is deflected by an AFM and the mechanical properties are extracted from the AFM data based on the (continuum) beam bending theory. In the contact mode, a suspended specimen is deflected vertically. It can be implemented in two ways: (1) the deflection at a particular position as

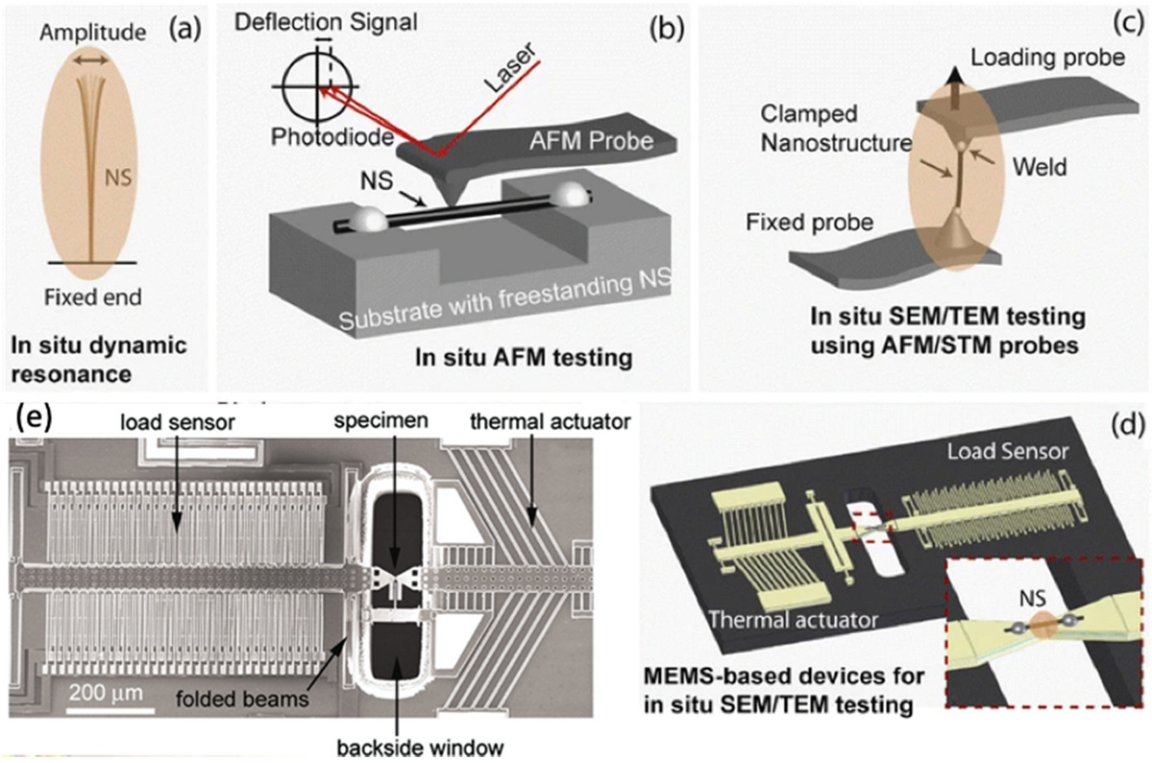

Fig. 1 Schematics of (a) resonance test, (b) AFM bending test in contact mode, (c) tension test using AFM probes, and (d) a MEMS device for tensile testing. (e) SEM image of the MEMS device for tensile testing. Reproduced from (d) Agrawal, R., Loh, O., Espinosa, H.D., 2011b. The evolving role of experimental mechanics in 1-D nanostructure-based device development. Experimental Mechanics 51, 1–9. (e) Zhu, Y., Espinosa, H.D., 2005. An electromechanical material testing system for in situ electron microscopy and applications. Proceedings of the National Academy of Sciences of the United States of America 102 (41), 14503–14508.

a function of the applied force, and (2) the deflection profile of the entire NW by scanning the AFM tip along its length at a constant force. The contact mode gained popularity, starting with mechanical testing of CNTs (Salvetat *et al.*, 1999), and later for a variety of NWs such as Si, Ag, ZnO, LaB_6 and amorphous SiO_2 (Paulo *et al.*, 2005; Jing *et al.*, 2006; Ni and Li, 2006; Ni *et al.*, 2006; Zhang *et al.*, 2008).

In the lateral force mode, two common sample configurations exist, either lying on a substrate with one end pinned or suspended over a trench with both ends pinned. In this mode, the load and deflection are obtained similar to the contact mode, except using the lateral force instead of the vertical force. The lateral force mode has been used to test mechanical properties of CNTs and SiC NWs (Wong *et al.*, 1997), Au NWs (Wu *et al.*, 2005), Si NWs (Heidelberg *et al.*, 2006), ZnO NWs (Wen *et al.*, 2008) and Ge NWs (Ngo *et al.*, 2006). In general, the contact mode has better resolution in displacement and force than the lateral force mode, but has the challenge of slippage of the AFM tip off the NW sample.

Tension

Tensile testing is the most popular among all the mechanical testing methods at the large scale due to its capability of measuring a wide range of mechanical properties and simplicity in data reduction. However, it is the most challenging one at the nanoscale in terms of sample preparation and high-resolution measurement of force and displacement.

Ruoff and co-workers pioneered tensile testing of individual CNTs inside SEM (Yu *et al.*, 2000). Two AFM cantilevers (probes) were used in the test with a stiff and a compliant cantilever used as the actuator and the load sensor, respectively. Electron-beam induced deposition (EBID) of amorphous carbon was used to clamps an individual CNT at the two AFM tips. The stiff AFM cantilever (actuator) used in Ruoff's work can be replaced with an even stiffer and sharp tungsten probe; the probe, attached to a nanomanipulator, is commonly used to manipulate 1D nanostructures. Zhu *et al.* used such a probe to manipulate and then conduct tensile testing of Si NWs in SEM. A compliant AFM cantilever was used as the load sensor (Zhu *et al.*, 2009). Strain resolution of 0.03% (for a NW of 3 μm in length) and load resolution of 1 nN were achieved.

MEMS consist of micrometer-scale components but offer nanometer displacement and nano-Newton force resolutions, meeting the stringent requirements for nanomechanical testing. MEMS-based in-situ SEM/TEM testing of nanostructures (Zhu and Espinosa, 2005; Haque *et al.*, 2011; Zhu and Chang, 2015) has received much interest. Zhu and Espinosa have developed the first MEMS stage that includes an on-chip actuator and an electronic load sensor with a gap in between (Zhu and Espinosa, 2005; Zhu *et al.*, 2005; 2006; Espinosa *et al.*, 2007). Two types of MEMS actuators were used, thermal actuator for displacement control and comb-drive

actuator for force control; the electronic load sensor was based on differential capacitive sensing. A number of MEMS platforms have been developed for testing a wide variety of 1D nanostructures including CNTs and NWs (Zhang *et al.*, 2009, 2011; Ganesan *et al.*, 2010; Brown *et al.*, 2011; Steighner *et al.*, 2011; Chen *et al.*, 2012; Tsuchiya *et al.*, 2012; Yilmaz and Kysar, 2013).

MEMS-based in-situ TEM testing enables quantitative stress-strain measurement as well as simultaneous TEM observation of defect dynamics. This powerful experimental method, together with atomistic modeling, has significantly advanced our understanding of not only mechanical properties of NWs but also deformation mechanisms at the nanoscale (Ramachandramoorthy *et al.*, 2015; Cheng *et al.*, 2017; Yin *et al.*, 2019). This makes possible employing NWs to probe important deformation mechanisms such as dislocation-twin boundary (TB) interactions, brittle-to-ductile transition, and hydrogen embrittlement; NWs are indeed an ideal probe for this purpose due to their well-controlled defect structure and small size for high-resolution TEM observation. In addition to quasistatic tensile testing, MEMS platforms have enabled a variety of advanced mechanical characterizations, such as fatigue test (Hosseinian and Pierron, 2013), under displacement or force control with feedback (Li *et al.*, 2020), different temperatures (Chang and Zhu, 2013; Chen *et al.*, 2014), at high strain rates (Ramachandramoorthy *et al.*, 2016; Li *et al.*, 2020), and strain effect on electric conductivity (Bernal *et al.*, 2014) and thermal conductivity (Murphy *et al.*, 2014).

Sample Preparation

Manipulation and mounting of NW specimens with nanoscale resolution and high throughput is a critical step in nanomechanical testing of NWs. This step becomes particularly challenging for tensile testing. It can be achieved by "pick and place" using a manipulator inside SEM (Zhu and Espinosa, 2005). EBID of amorphous carbon or platinum is commonly employed to clamp the specimens.

Some as-synthesized crystalline NWs are vertically oriented on a substrate. Thus, direct measurement on such as-synthesized NWs could eliminate the sample preparation step and avoid ambiguous boundary condition. The lateral force mode of AFM was used to deflect vertically aligned ZnO NWs and determine the Young's modulus (Song *et al.*, 2005b). In addition, an electrostatic field was also used to stimulate ZnO NWs to resonance to measure the Young's modulus (Chen *et al.*, 2006a). These vertically aligned NWs form strong bonding with the substrate. Bending tests have been performed to determine the fracture strengths of Si NWs (Hoffmann *et al.*, 2006).

Importance of Boundary Conditions

Uncertainly of the boundary conditions is a major challenge for nanomechanical testing, including resonance (Qin *et al.*, 2012), AFM contact mode or lateral force mode (Chen *et al.*, 2006b), and tension (Murphy *et al.*, 2013). For NWs without clamps (e.g., by EBID of amorphous carbon or platinum), the boundary condition purely depends on van der Waals interactions between the sample and the substrate. Even with the clamps, they are relatively compliant compared to the NWs. To assess the boundary conditions in the AFM bending, one method is to probe the NW at multiple locations along the length to obtain the deflection profile. In the case without clamps, Chen *et al.* (2006b) found that for NWs with small diameters, the deflection profiles were fitted best with the fixed-fixed (doubly clamped) boundary condition; while for NWs with large diameters, the deflection profiles were fitted better with simply supported boundary condition. The stiffness of the EBID clamps was found to be comparable to that of inorganic NWs (Murphy *et al.*, 2013). As a result, significant errors can be introduced in measurements of strain under tension tests and hence the measured Young's modulus.

Using the resonance test, Zhu and co-workers studied the effect of clamping on the measured Young's modulus of ZnO NWs and provided a guideline on how to obtain the "fixed" boundary condition (Qin *et al.*, 2012). The NWs were clamped at one end by EBID of amorphous carbon for in-situ SEM resonance tests. EBID was repeated several times to deposit more amorphous carbon at the same location. The resonance frequency was found to increase with the increasing clamp size until approaching a constant value corresponding to the "fixed" boundary condition. The critical clamp size was given as a function of the NW diameter and NW Young's modulus.

Size Effect

The surface atoms can be elastically stiffer or softer than the bulk atoms (Zhou and Huang, 2004). The softening effect is primarily due to the bond loss (i.e., loss of neighboring atoms on the surface). In contrast, the stiffening effect can be attributed to the electron redistribution (often called bond saturation) (Zhou and Huang, 2004; Shim *et al.*, 2005). Another mechanism that contributes to the size effect in Young's modulus of NWs, especially metallic NWs, is bulk (or core) nonlinear elasticity (Liang *et al.*, 2005). For example, the interior compressive stress caused by the tensile surface stress in metallic NWs is large enough to induce a nonlinear increase in the Young's modulus of the bulk atoms. Which mechanism plays a more dominant role depends on a number of factors such as the bonding type, NW diameter, axial orientation, and side surface facets (Zhou and Huang, 2004; Liang *et al.*, 2005; Zhu, 2017). In addition, loading type plays an important role in the measured size effect in Young's modulus. For example, if the surface elasticity is the dominant mechanism, the elasticity size effect would be manifested more strongly under bending than under tension as the surface plays a greater role during bending (Xu *et al.*, 2010), as shown in **Fig. 2** in the case of ZnO NWs (Xu *et al.*, 2010). It is thus recommended to perform tests under different loading modes (e.g., tension and bending) to decipher the size effect in Young's modulus (Chang *et al.*, 2016).

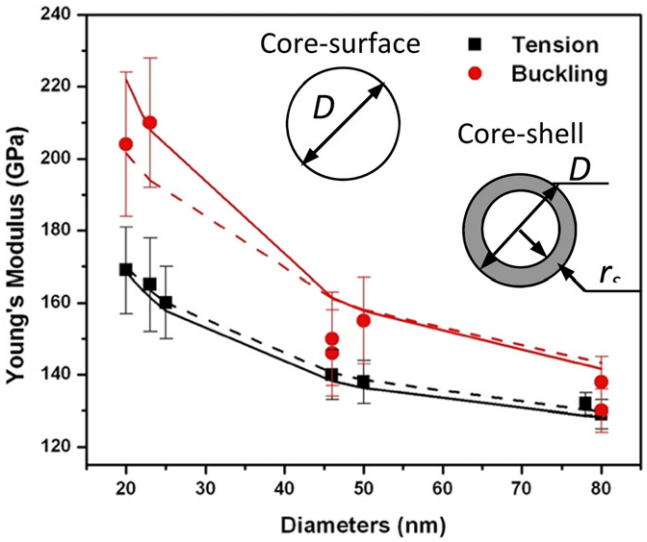

Fig. 2 The Young's modulus of ZnO NWs as a function of the NW diameter. The size effect is more pronounced under bending (buckling) than under tension. Reproduced from Xu, F., *et al.*, 2010. Mechanical properties of ZnO nanowires under different loading modes. Nano Research 3, 271–280.

Internal dislocation interaction is the dominant mechanism for plastic deformation of bulk materials. For NWs, however, dislocation nucleation from free surfaces becomes dominant (Park and Zimmerman, 2005; Park *et al.*, 2009; Zhu and Li, 2010; Weinberger and Cai, 2012; Zhu, 2017). As a result, the yield strength is expected to show sensitive temperature and strain-rate dependence and increase modestly with the decreasing NW diameter. Fracture is typically initiated from surface flaws (defects). But reports have also shown that it is possible to initiate fracture from internal defects such as point defects (He *et al.*, 2011). In either case, as the number of defects reduces with the decreasing NW size, the fracture strength increases.

Mechanical Properties of Metallic NWs

Metallic NWs have been synthesized by a range of methods, including the template method (Bera *et al.*, 2004), hydrothermal method (Liu *et al.*, 2003), electrochemical deposition (Tian *et al.*, 2003), chemical vapor deposition (Kim *et al.*, 2008), physical vapor deposition (Richter *et al.*, 2009; Yoo *et al.*, 2010), and polyol method (solution phase) (Murphy and Jana, 2002; Sun *et al.*, 2002; Wiley *et al.*, 2005; Wiley *et al.*, 2007). The last two methods are known to produce high-quality single-crystalline and penta-twinned NWs, respectively, with uniform diameter, smooth surfaces, and well-defined defect structures if any (e.g., TBs). Note that a penta-twinned NW has five twin segments joined along a common quintuple line in the axial direction. It is important to emphasize that high-quality NWs are extremely important for mechanical testing because it is critical to not only measure true mechanical properties but also to understand the deformation mechanisms. Among the many metallic NWs, Ag and Au NWs have received most attention. Studies on mechanical properties of metallic NWs focus on the elastic modulus, yield strength, ultimate strength, and plasticity. This section will begin by the mechanical properties of Ag and Au NWs considering the effect of NW size (diameter), planar defects, and cross-sectional shape, followed by several other metallic NWs (e.g., Cu, Ni and Pd).

Ag NWs

Young's modulus

The Young's modulus of Ag NWs has been extensively investigated by the resonance, bending, or tensile test. Most data showed a stiffening size effect in the Young's modulus, i.e., increasing from the bulk value of 84 GPa to about 180 GPa with the decreasing diameter (**Fig. 3**(a)) (Cuenot *et al.*, 2004; Jing *et al.*, 2006; Wu *et al.*, 2006; Filleter *et al.*, 2012; Zhu *et al.*, 2012; Alducin *et al.*, 2016; Chang *et al.*, 2016). For example, a study on penta- (or fivefold) twinned Ag NWs with $<110>$ orientation revealed a stiffening size effect in the Young's modulus between 34 and 130 nm in diameter (Zhu *et al.*, 2012). The Young's modulus continuously increased with the decreasing diameter below 80 nm and remained constant for diameter above 80 nm (close to the bulk value).

To decipher the mechanisms of the reported size effect in Young's modulus (surface elasticity or bulk nonlinear elasticity), Zhu and co-workers tested the same Ag NWs using two different methods, in situ SEM resonance test and tensile test. It was found that some combination of bulk nonlinear elasticity and surface elasticity is responsible for the measured size effect in Young's modulus of penta-twinned Ag NWs. In addition, the authors found a transition in the cross-sectional shape from pentagon to circle with decreasing NW diameter, which is of important relevance to quantify the size effect in Young's modulus (Chang *et al.*, 2016).

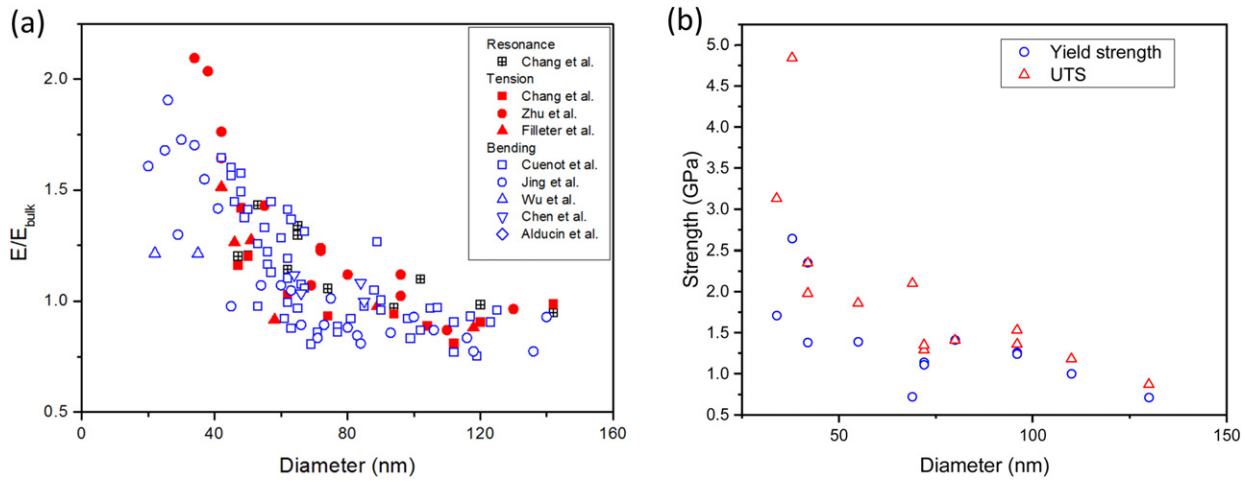

Fig. 3 (a) Size-dependent Young's modulus of Ag NWs. The data are normalized by the Young's modulus of bulk Ag in the $< 110 >$ direction. (b) Size-dependent yield strength and UTS of penta-twinned Ag NWs. Reproduced from (a) Cuenot, S., *et al.*, 2004. Surface tension effect on the mechanical properties of nanomaterials measured by atomic force microscopy. Physical Review B 69, 165410. Jing, G.Y., *et al.*, 2006. Surface effects on elastic properties of silver nanowires: contact atomic-force microscopy. Physical Review B 73, 235409. Wu, B., *et al.*, 2006. Microstructure-hardened silver nanowires. Nano Letters 6 (3), 468–472. Filleter, T., *et al.*, 2012. Nucleation-controlled distributed plasticity in penta-twinned silver nanowires. Small 8 (19), 2986–2993. Available at: https://doi.org/10.1002/smll.201200522. Zhu, Y., *et al.*, 2012. Size effects on elasticity, yielding and fracture of silver nanowires: In situ experiments. Physical Review B 85, 45443. Alducin, D., *et al.*, 2016. In situ transmission electron microscopy mechanical deformation and fracture of a silver nanowire. Scripta Materialia 113, 63–67. Available at: https://doi.org/10.1016/j.scriptamat.2015.10.011. Chang, T.-H., *et al.*, 2016. On the size-dependent elasticity of penta-twinned silver nanowires. Extreme Mechanics Letters 8, 177–183. Available at: https://doi.org/10.1016/j.eml.2016.03.007.

Strengths

Not like the Young's modulus, the yield strength and ultimate tensile strength of Ag NWs have been studied to a less extent. **Fig. 3** (b) shows the results from a systematic study (Zhu *et al.*, 2012; Narayanan *et al.*, 2015), where a total of 13 penta-twinned Ag NWs were tested under tension. The yield strength was found to be strongly size dependent, increasing from 0.71 to 2.64 GPa as the diameter decreased from 130 down to 34 nm. Yielding is a result of dislocation nucleation from the NW free surface. The highest yield strength of Ag NWs was about 50 times higher than that of bulk Ag (54 MPa), close to the theoretical tensile strength of Ag in the $\langle 110 \rangle$ direction – 3.5 GPa considering the (111)/(112) slip system. The ultimate tensile strength was also size dependent and generally higher than the yield strength, exhibiting strain hardening of the Ag NWs. The strain hardening was also size dependent; more specifically, Ag NWs with smaller diameters showed more hardening and higher ductility (Narayanan *et al.*, 2015). The size-dependent strain hardening was attributed to the obstruction of surface-nucleated dislocations by TBs.

Plastic behaviors

Twining and dislocation slip are two competitive deformation mechanisms in face-centered cubic (FCC) metals. The rivalry between the two mechanisms prevail in FCC metallic NWs, depending on the axial orientation (Schmid factor) and the generalized stacking fault energies (Weinberger and Cai, 2012). In NWs both mechanisms start with partial dislocation nucleation from free surfaces. Yin *et al.* (2019) recently found another factor, cross-sectional shape, may influence the competition between the two mechanisms in single-crystalline Ag NWs using in-situ TEM tensile testing and molecular dynamics (MD) simulations, as shown in **Fig. 4**. Twin deformation accompanied by a large plasticity occurred in NWs with low aspect ratios. With increasing aspect ratio, a transition in deformation mode from twinning to dislocation slip was observed. Theoretical and numerical studies showed that the energy barrier for twinning depends on the aspect ratio of the cross section, proportional to the change in surface energy as a result of the twinning-induced crystal reorientation. Larger aspect ratio would lead to larger increase in surface energy, causing suppression of twinning.

For NWs containing internal TBs, dislocations nucleated from free surfaces interact with TBs, leading to interesting mechanical behaviors such as recoverable plasticity and strain hardening. In the case of bi-twinned Ag NWs (with a single TB parallel to the NW axis), partial dislocations can be hindered by the TB, and upon unloading all or part of the partial dislocations retract from the TB, leading to full or partial plastic strain recovery, respectively (**Fig. 5**(a)) (Cheng *et al.*, 2020). The bi-twinned Ag NWs can also undergo stress relaxation, as a result of dislocation nucleation (**Fig. 5**(b)) (Cheng *et al.*, 2020). Under larger loading, the partial dislocations can transmit across the TB, leading to localized dislocation slip or necking and eventual fracture. However, when the volume ratio between the two twin variants is small, another deformation mechanism – detwinning of the existing TB – could occur (Cheng *et al.*, 2017), which can result in the twinning behavior similar to that reported in single-crystalline Ag NWs (Yin *et al.*, 2019).

For penta-twinned Ag NWs, stress relaxation and plastic strain recovery were also observed, similar to the bi-twinned Ag NWs but to a larger extent (**Fig. 5**(c) and (d)). The inhomogeneous stress field generated intrinsically by the fivefold twin structure can further drive the partial dislocations back upon unloading (Bernal *et al.*, 2015; Qin *et al.*, 2015). The TBs confine dislocation activities with a direct impact on ductility and strength by forming a complicated 3D dislocation structure (Filleter *et al.*, 2012;

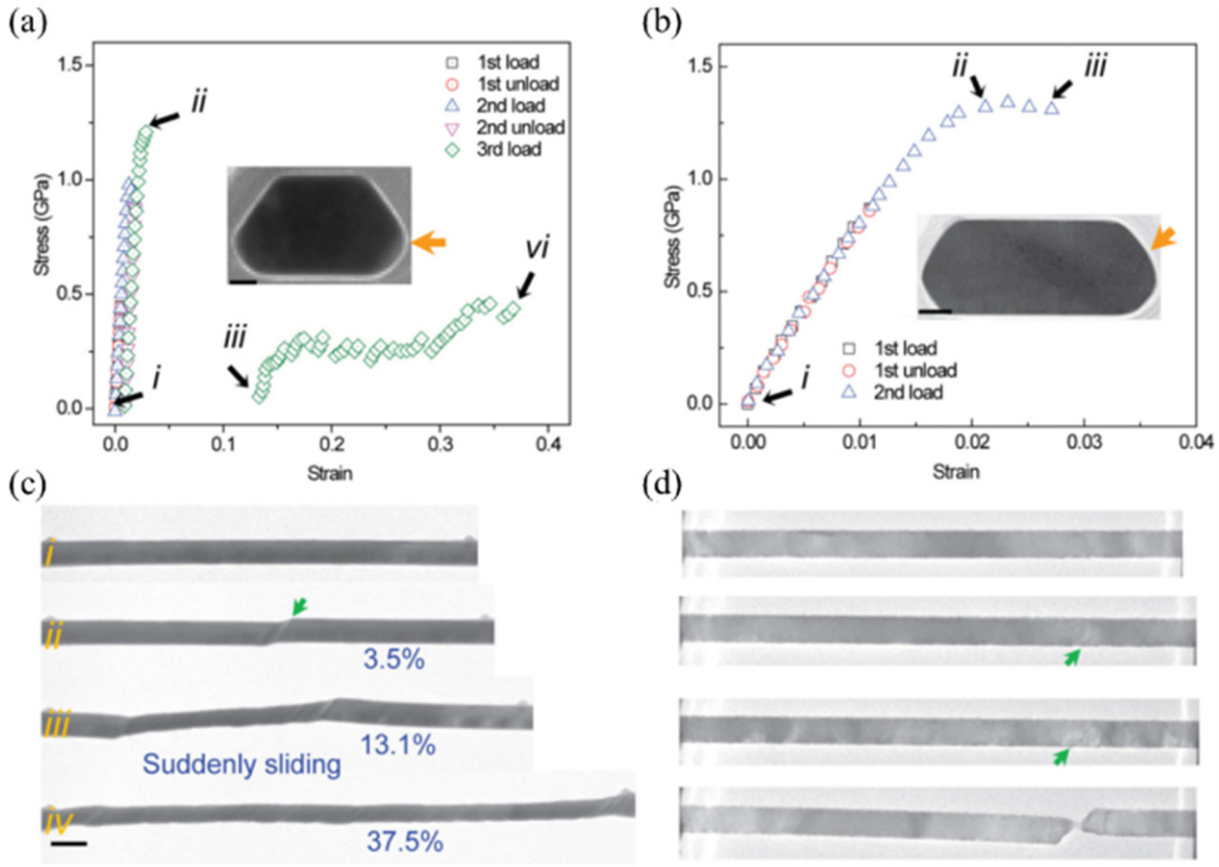

Fig. 4 Engineering stress–strain curves of two single-crystalline Ag NWs with different aspect ratios. Reproduced from Yin, S., Cheng, G., Richter, G., *et al.*, 2019. Transition of deformation mechanisms in single-crystalline metallic nanowires. ACS Nano 13 (8), 9082–9090. Available at: https://doi.org/10.1021/acsnano.9b03311.

Narayanan *et al.*, 2015). MEMS-based tensile testing was used to study the influence of strain rate on the deformation of Ag NWs. Brittle fracture was observed at low strain rates, while ductile fracture at high strain rates (Ramachandramoorthy *et al.*, 2016).

Au NWs

Different from Ag NWs, the reported Young's moduli of Au NWs are rather scattered. The average Young's modulus of Au NWs with diameter ranging from 40 to 250 nm measured by AFM bending was 70 ± 11 GPa (Wu *et al.*, 2005), close to the value of bulk Au (78 GPa). Resonance tests of single crystalline <100> Au NWs found a decrease in Young's modulus with decreasing NW diameter (Petrova *et al.*, 2006).

For yield strength and UTS of Au NWs, size effect was widely reported. As shown in **Fig. 6**(a), an increase in the yield strength from 200 MPa – bulk value of the yield strength – to as high as 8 GPa with a reduction of diameter from 300 to 40 nm was reported (Wu *et al.*, 2005; Lu *et al.*, 2011; Seo *et al.*, 2011; Sedlmayr *et al.*, 2012; Wang *et al.*, 2013). Single crystalline Au NWs, synthesized by physical vapor deposition, exhibited large plastic deformation as a result of coherent twin propagation as revealed by in-situ SEM tensile tests (Seo *et al.*, 2011; Sedlmayr *et al.*, 2012). The flow stress increased with the decreasing NW diameter (Seo *et al.*, 2013). The twinning-induced plastic deformation was reversible through a detwinning process under cyclic loading (Lee *et al.*, 2014). A size-dependent transition from dislocation plasticity to deformation twinning was observed in Au NWs (Hwang *et al.*, 2015). In addition to size, the transition was found to depend on the aspect ratio of the NW cross section, similar to the case of Ag NWs (Yin *et al.*, 2019). For <111> oriented Au NWs with angstrom-scale twins (TBs perpendicular to the NW axial direction), UTS was found to approach the theoretical limit (Wang *et al.*, 2013).

Other Metallic NWs

For metallic NWs, the elastic deformation is limited by the dislocation nucleation. Since single crystalline NWs are free of defects and large surface to volume ratio so they can sustain much higher elastic strain than the bulk ones. As a result of size reduction, a transition from ductile to brittle fracture in metallic NWs was found (Richter *et al.*, 2009). When the Cu NW diameter decreased

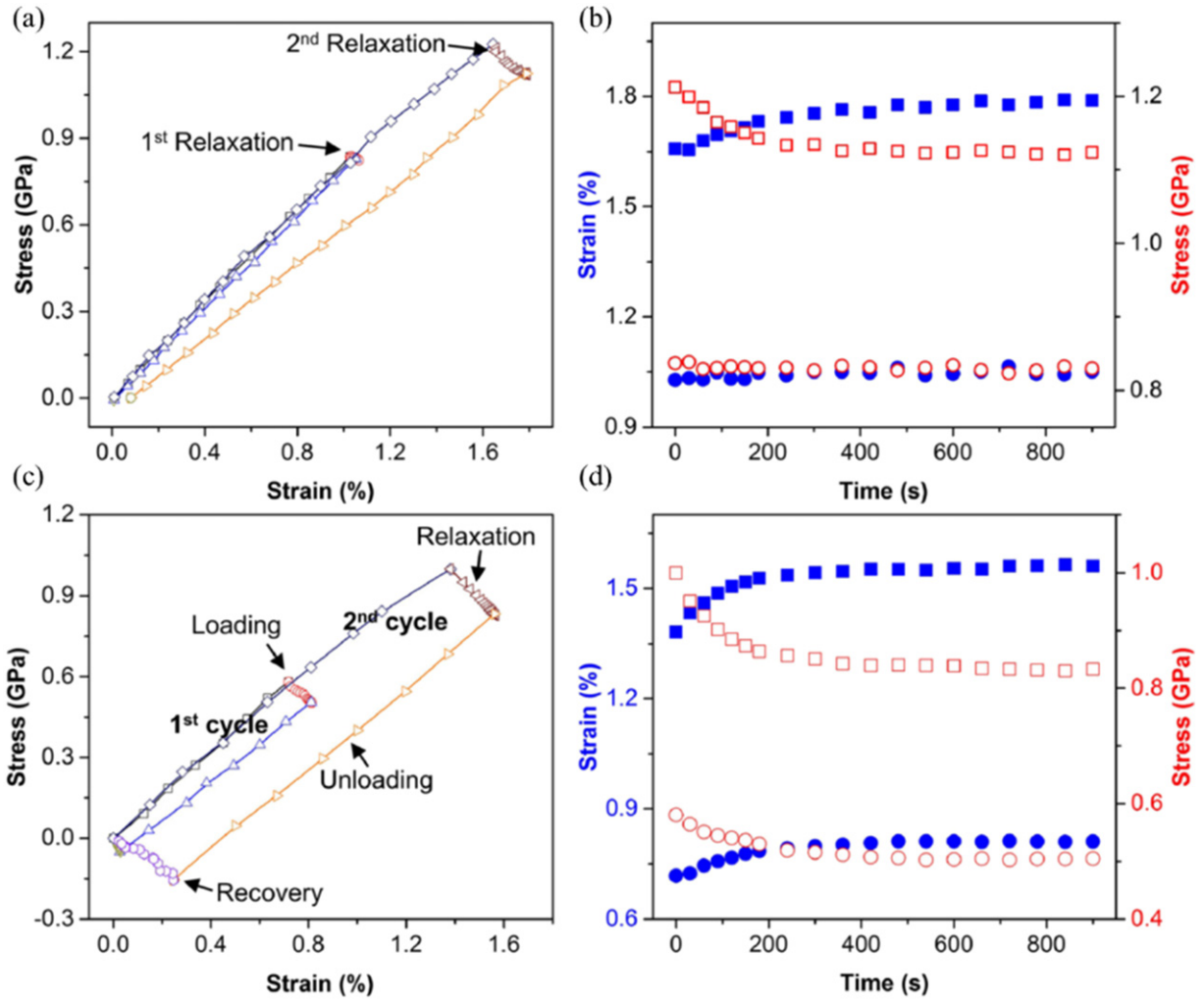

Fig. 5 In-situ measurements of stress and strain evolutions in bi- (a,b) and penta-twinned (c,d) Ag NWs. (a,c) Stress–strain curves for the bi- and penta-twinned NWs under two cycles of loading-relaxation-unloading-recovery, respectively. The relaxation and recovery steps took 15 min (b,d) Relaxation curves for the bi- and penta-twinned NWs, respectively. Solid and open symbols correspond to the strain-time and stress-time relationships, respectively. Square and circle symbols to high and low initial stress levels, respectively. Reproduced from Cheng, G., *et al.*, 2020. In-situ TEM study of dislocation interaction with twin boundary and retraction in twinned metallic nanowires. Acta Materialia 196, 304–312. Available at: https://doi.org/10.1016/j.actamat.2020.06.055. Qin, Q., *et al.*, 2015. Recoverable plasticity in penta-twinned metallic nanowires governed by dislocation nucleation and retraction. Nature Communications 6, 5983. Available at: https://doi.org/10.1038/ncomms6983.

from 300 to 75 nm, the tensile strength increased from 1 to 7 GPa, where the Cu NWs were synthesized by physical vapor deposition along <110> direction. **Fig. 6**(b) summarizes the strength data of the Cu NWs and the microwhiskers tested by Brenner back in the 50 s (Brenner, 1956).

The critical resolved shear stress of single crystalline Ni NWs was shown to increase with the decreasing nanowires diameter (Peng *et al.*, 2012). By electrochemical deposition on nanoporous anodic aluminum oxide (AAO) templates, Ni NWs with varying diameters (100–300 nm) were synthesized. In-situ SEM tensile tests were used to investigate the size and strain-rate dependency on the yield strength of <111> and <112> oriented Ni NWs. The yield strength increased from 1.2 to 3.4 GPa as the diameter decreased from 300 to 80 nm, while increased from 2 to 3 GPa as the strain rate increased from 10^{-4} to 10^{-2} s^{-1} for Ni NWs of 100 nm in diameter (Peng *et al.*, 2013).

Pd NWs, synthesized by physical vapor deposition (<110> oriented), displayed nonlinear elasticity beyond 1% strain. The Young's modulus increased from 120 GPa for NWs larger than 100 nm in diameter to 290 GPa for NWs of 33 nm in diameter from in-situ SEM tensile testing (Chen *et al.*, 2012). As the diameter of the single crystalline Pd NWs decreased from 260 to 40 nm, the yield strength increased from 1 to 4 GPa. While it is generally known that the tensile stress required to nucleate partial dislocations from the surface increases as the NW diameter decreases, Chen *et al.* reported that defect-free Pd NWs exhibit an apparent stochasticity in the measured strength of dislocation nucleation, which was attributed to a thermally activated deformation process (Chen *et al.*, 2015). This work, along with others, revealed that the yield strength only shows a modest size effect in defect-free NWs.

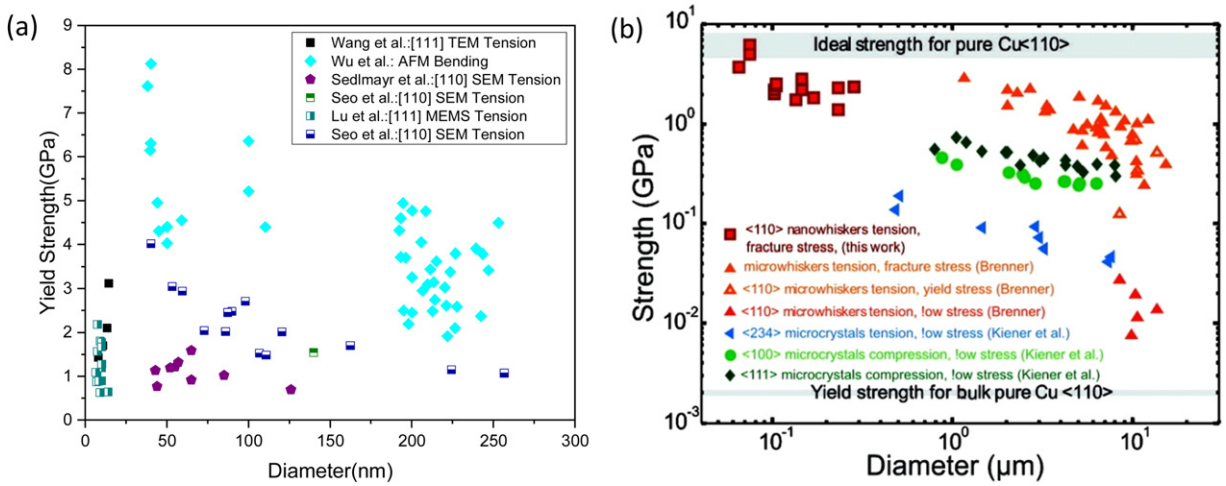

Fig. 6 Size effect on the yield strength of (a) Au and (b) Cu NWs. Reproduced from (a) Wu, B., Heidelberg, A., Boland, J.J., 2005. Mechanical properties of ultrahigh-strength gold nanowires. Nature Materials 4 (7), 525–529. Available at: isi:000230190900014. Lu, Y., *et al.*, 2011. Surface dislocation nucleation mediated deformation and ultrahigh strength in sub-10-nm gold nanowires. Nano Research 4 (12), 1261–1267. Available at: https://doi.org/10.1007/s12274-011-0177-y. Seo, J.-H., *et al.*, 2011. Superplastic deformation of defect-free Au nanowires via coherent twin propagation. Nano letters 11 (8), 3499–3502. Available at: https://doi.org/10.1021/nl2022306. Sedlmayr, A., *et al.*, 2012. Existence of two twinning-mediated plastic deformation modes in Au nanowhiskers. Acta Materialia 60 (9), 3985–3993. Available at: https://doi.org/10.1016/j.actamat.2012.03.018. Wang J. *et al.*, 2013. Near-ideal theoretical strength in gold nanowires containing angstrom scale twins. Nature communications 4, 1742. Available at: https://doi.org/10.1038/ncomms2768. (b) Richter, G., *et al.*, 2009. Ultra high strength single crystalline nanowhiskers grown by physical vapor deposition. Nano Letters 9, 3048–3052.

The authors hypothesized that diffusion of point defects is the origin of the surface dislocation nucleation. The exact nature of the diffusion process and its influence on dislocation nucleation, however, remain elusive and warrant further investigation.

Mechanical Properties of Ionic NWs

ZnO NWs

Young's modulus

Due to the large exciton binding energy and wide bandgap, ZnO is an important semiconducting, piezoelectric and biocompatible materials (Wang, 2003). The Young's modulus of ZnO NWs has been extensively investigated, as summarized in **Fig. 7**(a). AFM based lateral bending of vertical aligned ZnO NWs showed that the Young's modulus of ZnO NWs with an average diameter of 45 nm is 29 $\pm$ 8 GPa (Song *et al.*, 2005b), which is significantly lower than the bulk value (140 GPa). Wen *et al.* reported that Young's modulus of ZnO NWs is independent of diameter and close to the bulk value, for the NWs ranging from 18 to 304 nm in diameter. However, Chen *et al.* (2006a) reported a size dependence of Young's modulus in [0001] oriented ZnO NWs using electric-field-induced resonance in SEM. The measured values were up to 220 GPa for diameter of 17 nm. Agrawal *et al.* (2008) reported a similar size effect using in-situ TEM tension testing, which was supported by their MD simulations. Xu *et al.* conducted in-situ SEM tension and buckling test on the same [0001] ZnO NWs and found that the tensile modulus and bending modulus increased when the NW diameter decreased from 80 to 20 nm. Interestingly, the bending modulus increased faster than the tensile modulus, indicating that the elasticity size effect in ZnO NWs is mainly due to surface stiffening. A core-shell model based on continuum mechanics was used to fit the experimental data well (Xu *et al.*, 2010).

Fracture strength

Size dependency of the fracture strength of ZnO NWs has been reported, see **Fig. 7**(b). Desai *et al.* reported a considerable increase in the fracture strength from 5 to 15 GPa with a decrease in NW diameter from 500 to 200 nm (Desai and Haque, 2007). Xu *et al.* (2010) found a similar rise in strength from 4 to 10 GPa when the NW diameter decreased from 90 to 20 nm. According to Agrawal *et al.* (2008) and Wen *et al.* (2008) a diameter decrease from 500 to 20 nm resulted in a rise in the fracture strength from 3 to 10 GPa. Tensile and bending measurements were used to determine the fracture strength of [0001] oriented ZnO NWs vertically synthesized on a sapphire substrate, with diameters ranging from 60 to 310 nm (Hoffmann *et al.*, 2007). The tensile strength was 3.7–5.5 GPA, while the bending strength was found to be approximately twice as large as the tensile fracture strength.

To understand the size effect in the fracture strength, two hypotheses, based on surface flaws and internal defects (point defects), have been proposed. According to Weibull statistics, a correlation between the surface area and the fracture strength was identified, implying that surface flaws are responsible for the NW fracture (Agrawal *et al.*, 2008). However, He *et al.* (2011) found a

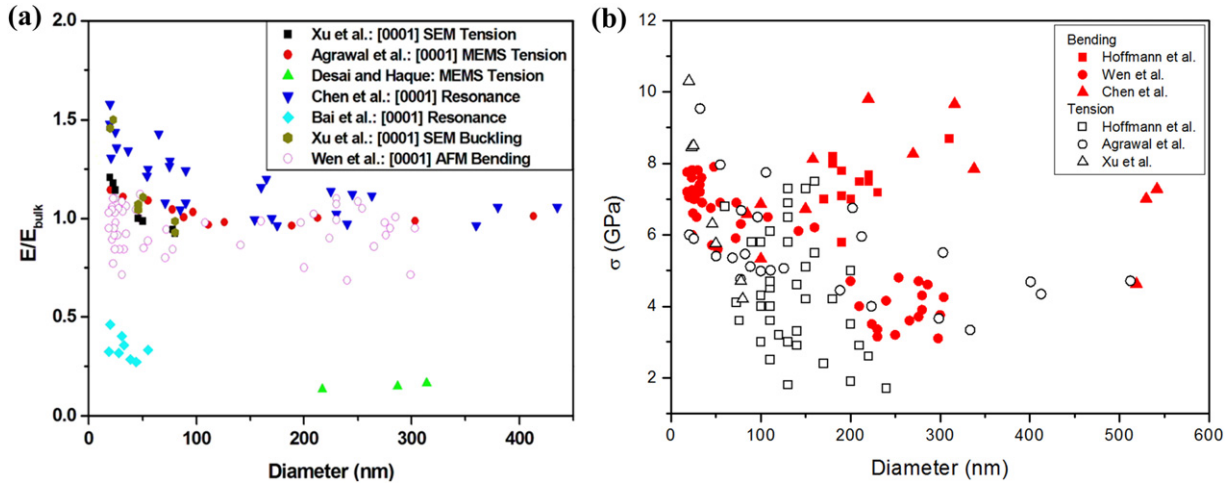

Fig. 7 (a) Size effect on Young's modulus of ZnO NWs. (b) Size effect on fracture strength of ZoO NWs. Reproduced from (a) Bai, X.D., *et al.*, 2003. Dual-mode mechanical resonance of individual ZnO nanobelts. Applied Physics Letters 82 (26), 4806–4808. Chen, C.Q., *et al.*, 2006a. Size dependence of the Young's modulus of ZnO nanowires. Physical Review Letters 96, 75505. Desai, A.V., Haque, M.A., 2007. Mechanical properties of ZnO nanowires. Sensors and Actuators a-Physical 134 (1), 169–176. Agrawal, R., *et al.*, 2008. Elasticity size effects in ZnO nanowires - a combined experimental-computational approach. Nano Letters 8 (11), 3668–3674. Wen, B., Sader, J.E., Boland, J.J., 2008. Mechanical properties of ZnO nanowires. Physical Review Letters 101, 175502. Xu, F., *et al.*, 2010. Mechanical properties of ZnO nanowires under different loading modes. Nano Research 3, 271–280. (b) Chen, C.Q., Zhu, J., 2007. Bending strength and flexibility of ZnO nanowires. Applied Physics Letters 90 (4), 043105. Hoffmann, S., *et al.*, 2007. Fracture strength and Young's modulus of ZnO nanowires. Nanotechnology 18 (20), 205503. Agrawal, R., Peng, B., Espinosa, H.D., 2009. Strength and fracture mechanism of zinc oxide nanowires under uniaxial tensile load. Nano Letters 9, 4177–4183. Xu, F., *et al.*, 2010. Mechanical properties of ZnO nanowires under different loading modes. Nano Research 3, 271–280.

correlation between the volume and the fracture strength, also using Weibull statistics, which indicates that the NW fracture is due to internal (volume) defects. The authors used in-situ cathodoluminescence (CL) analysis to confirm the presence of vacancies in the ZnO NWs. The fracture behavior of ZnO NWs is possibly a result of both surface defects and internal point defects. However, quantifying the contribution of each type of defect remains challenging due to the difficulty of quantifying the density and distribution of such defects, particularly point defects. A potential method is atom probe tomography (APT) that can determine the density and distribution of point defects down to the single-atom level. APT's local electrode atom probe (LEAP) technology has been demonstrated on single NWs (Agrawal *et al.*, 2011a).

Anelasticity

Zhu and co-workers *et al.* discovered a giant anelasticity in ZnO and doped Si NWs using in-situ SEM bending tests. For a single NW, upon removal of the bending load, a substantial portion of the total strain gradually recovers following instantaneous recovery of the elastic strain (Cheng *et al.*, 2015). Such an anelasticity was attributed to point defect diffusion in an inhomogeneous strain field. The presence of point defects was confirmed by the electron energy loss spectroscopy. This work is another manifestation that point defects could play an increasingly important role on the mechanical properties of nanostructures.

GaN and GaAs NWs

Gallium nitride (GaN), a significant semiconductor with a wide direct band gap of 3.4 eV at room temperature, is of particular interest due to its potential application in blue and ultraviolet light emitters as well as high temperature and high power optoelectronic devices (Liu *et al.*, 2005). Nam *et al.* (2006) determined the diameter-dependent Young's modulus of GaN NWs via in-situ electromechanical resonance tests in TEM. The measured Young's modulus was close to the theoretical value of bulk GaN (300 GPa) at the largest diameter studied (84 nm) and steadily decreased with the decreasing diameter. Planar defects such as SFs were found to influence the Young's modulus of GaN NWs considerably (Dai *et al.*, 2015). The tensile fracture strength of GaN NWs was determined to be in the region of 4–7 GPa using MEMS tensile testing (Brown *et al.*, 2011). Cyclic tensile tests found that single crystalline GaN NWs were capable of withstanding uniaxial strains of at least 0.01 and up to 0.04.

Using in-situ TEM compression test, Wang *et al.* studied the mechanical behavior of vertically aligned single crystalline $<111>$-oriented GaAs NWs grown on a GaAs substrate (Wang *et al.*, 2011). For GaAs NWs with diameters ranging from 50 to 150 nm, the elastic strain limit was found to be 10%–11%. When the diameter was less than 25 nm, the GaAs NWs exhibited obvious plastic deformation. The Young's modulus of the NWs increased noticeably as the NW diameter decreased. The Young's moduli of GaAs NWs with two distinct structures, defect-free single crystalline wurtzite and defective wurtzite containing a high density of SFs, were investigated. The presence of a high density of SFs was found to increase the Young's modulus by 13% (Chen *et al.*, 2016).

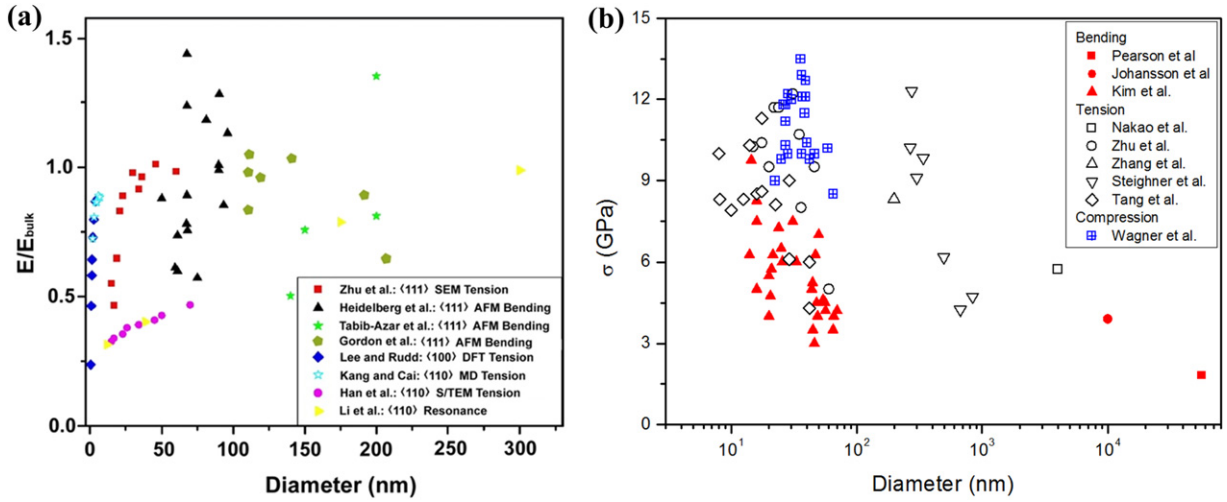

Fig. 8 (a) Size effect on Young's modulus of Si NWs. (b) Size effect on fracture strength of Si NWs. Reproduced from (a) Li, X.X., *et al.*, 2003. Ultrathin single-crystalline-silicon cantilever resonators: Fabrication technology and significant specimen size effect on Young's modulus. Applied Physics Letters 83 (15), 3081–3083. Tabib-Azar, M., *et al.*, 2005. Mechanical properties of self-welded silicon nanobridges. Applied Physics Letters 87, 113102. Heidelberg, A., *et al.*, 2006. A generalized description of the elastic properties of nanowires. Nano Letters 6 (6), 1101–1106. Han, X., *et al.*, 2007. Low-temperature in situ large-strain plasticity of silicon nanowires. Advanced Materials 19, 2112–2118. Kang, K., Cai, W., 2007. Brittle and ductile fracture of semiconductor nanowires - molecular dynamics simulations. Philosophical Magazine 87 (14–15), 2169–2189. Lee, B., Rudd, R.E., 2007. First-principles calculation of mechanical properties of Si nanowires and comparison to nanomechanical theory. Physical Review B 75, 195328. Gordon, M.J., *et al.*, 2009. Size effects in mechanical deformation and fracture of cantilevered silicon nanowires. Nano Letters 9 (2), 525–529. Available at: https://doi.org/10.1021/n1802556d. Zhu, Y., *et al.*, 2009. Mechanical properties of vapor-liquid-solid synthesized silicon nanowires. Nano Letters 9, 3934–3939. Pearson, G., Read, W., Feldmann, W., 1957. Deformation and fracture of small silicon crystals. Acta Metallurgica 5 (4), 181–191. Available at: https://doi.org/10.1016/0001-6160(57)90164-5. Johansson, S., *et al.*, 1998. Fracture testing of silicon microelements in situ in a scanning electron microscope. Journal of Applied Physics 63 (10), 4799–4803. Available at: https://doi.org/10.1063/1.340471. Nakao, S., *et al.*, 2006. Mechanical properties of a micron-sized SCS film in a high-temperature environment. Journal of Micromechanics and Microengineering 16 (4), 715–720. Zhang, D., *et al.*, 2010. In situ electron microscopy mechanical testing of silicon nanowires using electrostatically actuated tensile stages. Journal of Microelectromechanical Systems 19 (3), 663–674. Available at: https://doi.org/10.1109/JMEMS.2010.2044746. Kim, Y.-J., *et al.*, 2011. Exploring nanomechanical behavior of silicon nanowires: AFM bending versus nanoindentation. Advanced Functional Materials 21 (2), 279–286. Available at: https://doi.org/10.1002/adfm.201001471. Steighner, M.S., *et al.*, 2011. Dependence on diameter and growth direction of apparent strain to failure of Si nanowires. Journal of Applied Physics, 109 (3), 033503. doi: 03350310.1063/1.3537658. Tang, D.-M., *et al.*, 2012. Mechanical properties of Si nanowires as revealed by in situ transmission electron microscopy and molecular dynamics simulations. Nano letters 12 (4), 1898–1904. Available at: https://doi.org/10.1021/nl204282y. Wagner, A., *et al.*, 2015. Mechanisms of plasticity in near-theoretical strength sub-100 nm Si nanocubes. Acta Materialia 100, 256–265.

Mechanical Properties of Covalent NWs

Si NWs

Young's modulus

Si is one of the most important materials in the semiconductor and MEMS industries. Si NWs exhibits unique mechanical, electrical, and optical capabilities with potential applications in mechanical oscillators, sensors, field effect transistors, photovoltaics, and lithium ion batteries. Young's modulus as a function of diameter for Si NWs size is summarized in **Fig. 8**. Li *et al.* (2003) reported a size effect on Young's modulus of single crystalline silicon cantilevers (12–170 nm) by resonance measurement; Young's modulus decreases monotonously as the cantilevers becomes thinner. Zhu *et al.* (2009) reported stress–strain measurements of Si NWs (diameter range 15–60 nm) using in-situ SEM tensile testing. The Si NWs were synthesized using the vapor-liquid-solid (VLS) mechanism. When the diameters of Si NWs were larger than 30 nm, the Young's modulus was close to the bulk value (e.g., 187 GPa for $<111>$ orientation). However, when the diameters were less than 30 nm, the softening tendency became clear, i.e., the Young's modulus decreases with the decreasing NW diameter. On the other hand, some studies reported a stiffening effect with the decreasing diameter (Tabib-Azar *et al.*, 2005; Gordon *et al.*, 2009; Tsuchiya *et al.*, 2018). In addition to surface elasticity, the observed size effect in Young's modulus could be related to the presence of native oxide and surface imperfections.

Fracture

Numerous studies have been reported on the fracture strength of Si NWs. In general, fracture strength of Si NWs increases as the diameter decreases as shown in **Fig. 8**(b) (Pearson *et al.*, 1957; Johansson *et al.*, 1988; Nakao *et al.*, 2006; Zhu *et al.*, 2009; Zhang *et al.*, 2010; Kim *et al.*, 2011; Steighner *et al.*, 2011; Tang *et al.*, 2012; Wagner *et al.*, 2015). Zhu *et al.* (2009) found that the fracture strength increases from 5.1 to 12.2 GPa and fracture strain increases from 2.7% to about 12%, as the NW diameter reduces from 60

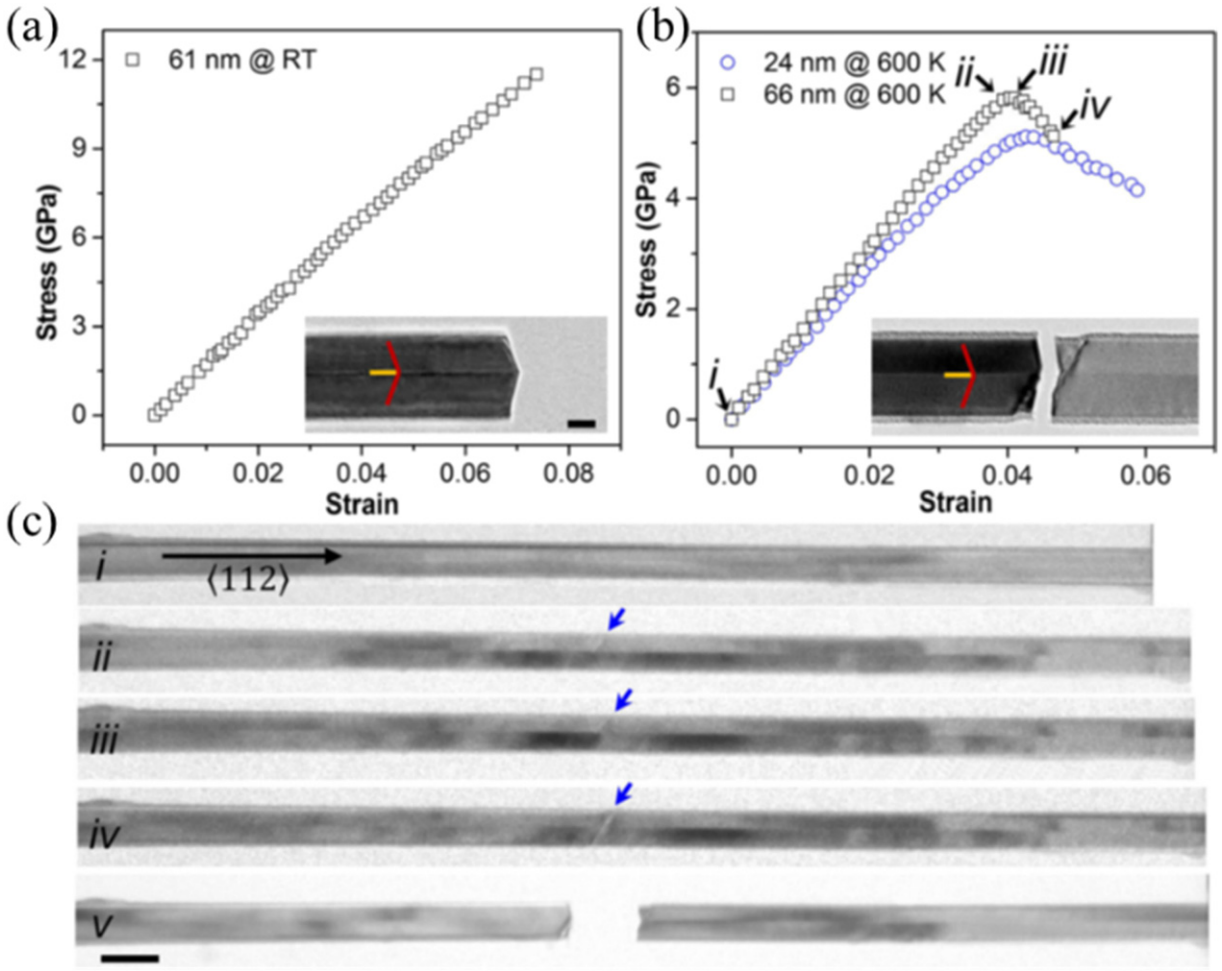

Fig. 9 In-situ MEMS-based tensile testing and TEM observation of mechanical behavior of Si NWs at room and elevated temperatures. (a,b) Stress–strain curves of Si NWs tested at 295 and 600K, respectively. Insets in (a,b) are the corresponding fracture morphologies of the tested NWs with diameters of 61 and 66 nm, respectively. Scale bar, 20 nm. (c) Snapshots of microstructure evolution corresponding to (b). Reproduced from (b) Cheng, G., *et al.*, 2019. In Situ Nano-thermomechanical Experiment Reveals Brittle to Ductile Transition in Silicon Nanowires. Nano Letters 19 (8), 5327–5334. Available at: https://doi.org/10.1021/acs.nanolett.9b01789.

to 15 nm. The measured value is close to the theoretical values of 15.2 and 18.8 GPa for Si in the <110> and <111> directions, respectively. The fracture of Si NWs was attributed to the surface flaws. Hoffmann *et al.* (2006) measured the bending strength of VLS-synthesized <111> -oriented Si NWs with diameters between 100 and 200 nm. The maximum bending strain before fracture was 6%, corresponding to a fracture strength of 12 GPa.

Brittle to ductile transition (BDT) has been extensively studied for bulk Si. However, it remains unclear how BDT in Si NWs is affected by the NW size and in particular if Si NWs become ductile at room temperature. A number of studies showed that Si NWs behave linear elastically until brittle fracture under tension (Gordon *et al.*, 2009; Zhu *et al.*, 2009; Tang *et al.*, 2012; Zhang *et al.*, 2016); by contrast, a few studies demonstrated that Si NWs could exhibit substantial plastic deformation under tension (Han *et al.*, 2007) and especially under bending (Tang *et al.*, 2012; Kang and Saif, 2013). Cheng *et al.* (2019) found that Si NWs are brittle at room temperature but exhibits ductile behavior with dislocation-mediated plasticity at elevated temperature by in-situ temperature-controlled nanomechanical tensile testing in TEM. 78 Si NWs were tested between room temperature and 600K, which revealed that unconventional ½<110> {001}dislocations become highly active with increasing temperature, resulting in the transition from brittle fracture to dislocation-mediated plasticity and ductile fracture at elevated temperature, as shown in **Fig. 9**.

SiC NWs

Utilizing AFM-based bending tests, Wong *et al.* (1997) first reported the fracture strength of SiC NWs. The maximum fracture strength of SiC NWs was 53.4 GPa, significantly higher than the values reported for bulk SiC and microscale SiC whiskers. Han *et al.* (2005) examined the plastic deformation behavior of intrinsically brittle SiC NWs by high resolution TEM. The plastic deformation was attributed to localized lattice bending, atomic lattice disordering, and amorphization.

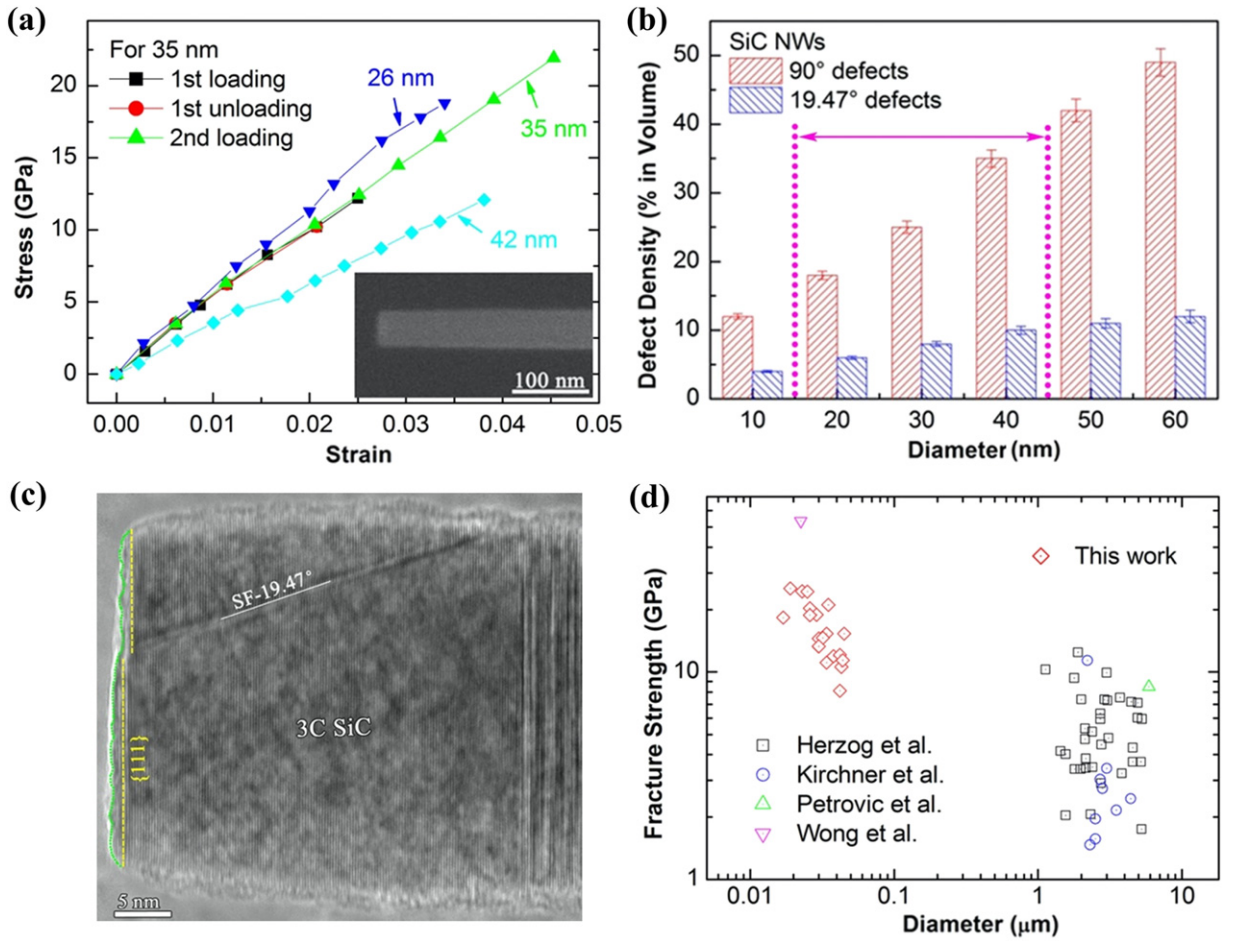

Fig. 10 (a) Representative tensile stress – strain curves of SiC NWs. (b) Defect density as a function of NW diameter. Here 90° and 19.47° defects refer to highly defective structures and 3C structures with a 19.47° SFs, respectively. (c) High-resolution TEM image of the fracture surface of a SiC NW. (d) Fracture strength of SiC NWs and whiskers as a function of the diameter. Reproduced from (d) Cheng, G., *et al.*, 2014. Mechanical properties of silicon carbide nanowires: Effect of size-dependent defect density. Nano Letters 14 (32), 754–758. Available at: https://doi.org/10.1021/nl404058r.

Cheng *et al.* (2014) reported the effect of size-dependent defect density of SiC NWs, consisting of pure 3C structure, 3C structure with an inclined SF, and highly defective structure. The SiC NWs, <111> -oriented, were synthesized by high-temperature thermal evaporation through the VLS process. In contrast to previously observed superplasticity, SiC NWs were found to fail in brittle fracture at ambient temperature (**Fig. 10**(a)). It is worth noting that cracks originate and propagate in the 3C segments with the 19.47° SFs, rather than in the highly defective segments. The size effect on the fracture strength of SiC NWs was related to the size-dependent defect density (i.e., the 3C structure with 19.47° SFs) (**Fig. 10**(b) and (c)). Internal structures and flaws are frequently present in both bottom-up and top-down produced crystalline NWs (in addition to free surfaces). This work emphasizes the critical importance of closely examining the interior structures and flaws of such NWs and their effect on the nanomechanical behavior. The fracture strength of SiC NWs displayed a strong size effect; that is, the fracture strength increased up to over 25 GPa with the decreasing diameter, close to the theoretical strength of 3C SiC (**Fig. 10**(d)).

Summary and Outlook

This article summarizes recent advances in the mechanical properties of NWs. Almost all the methods for mechanical characterization of NWs use different types of microscopes (TEM, SEM, or AFM) as a platform for seeing, manipulating, deforming and measuring the properties of NWs. Many aspects of the mechanical properties of NWs have been investigated, including elasticity, fracture, plasticity, and anelasticity, often in combination with atomistic simulations. In particular, significant progress in the experimental mechanics of NWs has been made possible by in-situ TEM testing, which enable direct dynamic observation of deformation processes and concurrent recording of stress–strain curves. Free surfaces and often times interior defects were shown to have a significant impact on the mechanical properties of NWs.

It is worth noting that much of the early work on mechanical property measurements revealed significant scatter and discrepancy, which is understandable given the field's infancy, the challenge of conducting such measurements, and the possibility of differences in the synthesis methods and hence the shape and microstructures of NW samples. For instance, the NW cross section may change with diameter, which may have a significant effect on the mechanical properties measured (Chang *et al.*, 2016). For this consideration, this article concentrates on representative data and underlying mechanisms. With continued advance in testing methods and careful consideration of the factors mentioned above, more consistent testing results have been and will continue to be obtained. For example, efforts have been taken on systematic examination of the effects of sample cross sections (Chang *et al.*, 2016) and microstructures (Wang *et al.*, 2013; Bernal *et al.*, 2015; Qin *et al.*, 2015), loading modes (Xu *et al.*, 2010; Chang *et al.*, 2016), and boundary conditions (Qin *et al.*, 2012; Murphy *et al.*, 2013).

Along with measurements of the basic mechanical properties (e.g., Young's modulus, yield strength, and fracture strength), advanced behaviors and deformation processes of NWs have gained increasing interest in recent years. Advanced behaviors are those that are dependent on the testing temperature, rate, time, and environment, among other variables, which are of direct relevance to applications of NWs. For example, hydrogen embrittlement of Ag NWs has been probed, which revealed that hydrogen can suppress the dislocation nucleation from NW surfaces, responsible for the observed hydrogen embrittlement (Yin *et al.*, 2019). Multiphysical properties of NWs are of increasing interest. Given the large elastic strain range of NWs, they are ideal candidates to tune other properties (e.g., electric, thermal, optical, catalytic) using elastic strain. MEMS-based techniques, due to their precise control, integrated actuation and sensing, multifunctionality, and compatibility with imaging tools like TEM, have shown promising potential in characterizing such advanced mechanical behaviors, deformation processes, and multiphysical properties.

With their outstanding mechanical properties, NWs have found a wide spectrum of applications related to the mechanical properties, such as flexible and stretchable electronics (Javey *et al.*, 2007; McAlpine *et al.*, 2007; Takei *et al.*, 2010; Xu *et al.*, 2011; Xu and Zhu, 2012; Zhou *et al.*, 2020), nanocomposites (Yang *et al.*, 2005), nanoelectromechanical systems (Li *et al.*, 2007; He *et al.*, 2008; Feng *et al.*, 2010), energy harvesting (Law *et al.*, 2005; Wang and Song, 2006; Boukai *et al.*, 2008; Hochbaum *et al.*, 2008), and energy storage (Chan *et al.*, 2008; Huang *et al.*, 2010). Understanding the mechanical properties plays a critical role in the reliability of such applications. Large-scale applications with NWs as the building blocks must be rigorously pursued in order to maintain the high level of interest in NWs and fulfill their promising potential. On the other hand, operation and reliability of such applications require further understanding of mechanical properties of NWs especially under different service conditions such as cyclic loading, high rate, high temperature and extreme environment.

Acknowledgment

We would like to gratefully acknowledge the financial support of the National Science Foundation (NSF) under Award Nos. 1762511 and 1929646.

References

Agrawal, R., *et al.*, 2008. Elasticity size effects in ZnO nanowires - a combined experimental-computational approach. Nano Letters 8 (11), 3668–3674.
Agrawal, R., *et al.*, 2011a. Characterizing atomic composition and dopant distribution in wide band gap semiconductor nanowires using laser-assisted atom probe tomography. The Journal of Physical Chemistry C 115 (36), 17688–17694. https://doi.org/10.1021/jp2047823. (American Chemical Society).
Agrawal, R., Loh, O., Espinosa, H.D., 2011b. The evolving role of experimental mechanics in 1-D nanostructure-based device development. Experimental Mechanics 51, 1–9.
Alducin, D., *et al.*, 2016. In situ transmission electron microscopy mechanical deformation and fracture of a silver nanowire. Scripta Materialia 113, 63–67. https://doi.org/10.1016/j.scriptamat.2015.10.011.
Belov, M., *et al.*, 2008. Mechanical resonance of clamped silicon nanowires measured by optical interferometry. Journal of Applied Physics 103, 7.
Bera, D., Kuiry, S.C., Seal, S., 2004. Synthesis of nanostructured materials using template-assisted electrodeposition. JOM 56 (1), 49–53. https://doi.org/10.1007/s11837-004-0273-5.
Bernal, R.A., *et al.*, 2014. In situ electron microscopy four-point electromechanical characterization of freestanding metallic and semiconducting nanowires. Small 10 (4), 725–733. https://doi.org/10.1002/smll.201300736.
Bernal, R.A., *et al.*, 2015. Intrinsic bauschinger effect and recoverable plasticity in pentatwinned silver nanowires tested in tension. Nano Letters 15 (1), 139–146. https://doi.org/10.1021/nl503237t. (American Chemical Society).
Boukai, A.I., *et al.*, 2008. Silicon nanowires as efficient thermoelectric materials. Nature 451 (7175), 168–171.
Brenner, S.S., 1956. Tensile strength of whiskers. Journal of Applied Physics 27 (12), 1484–1491. https://doi.org/10.1063/1.1722294.
Brown, J.J., *et al.*, 2011. Tensile measurement of single crystal gallium nitride nanowires on MEMS test stages. Sensors and Actuators A Physical 166 (2), 177–186. https://doi.org/10.1016/j.sna.2010.04.002. (Elsevier B.V.).
Chan, C.K., *et al.*, 2008. High-performance lithium battery anodes using silicon nanowires. Nature Nanotechnology 3 (1), 31–35.
Chang, T.-H., *et al.*, 2016. On the size-dependent elasticity of penta-twinned silver nanowires. Extreme Mechanics Letters 8, 177–183. https://doi.org/10.1016/j.eml.2016.03.007.
Chang, T.-H., Zhu, Y., 2013. A microelectromechanical system for thermomechanical testing of nanostructures. Applied Physics Letters 103 (26), 263114. https://doi.org/10.1063/1.4858962.
Chen, C.Q., *et al.*, 2006a. Size dependence of the Young's modulus of ZnO nanowires. Physical Review Letters 96. 75505.
Chen, Y., *et al.*, 2006b. On the importance of boundary conditions on nanomechanical bending behavior and elastic modulus determination of silver nanowires. Journal of Applied Physics 100 (10), 104301. https://doi.org/10.1063/1.2382265.
Chen, L., *et al.*, 2012. Lattice anharmonicity in defect-free Pd nanowhiskers. Physical Review Letters 109 (12), 125503. (American Physical Society). https://doi.org/10.1103/PhysRevLett.109.125503.
Chen, L.Y., *et al.*, 2014. Temperature controlled tensile testing of individual nanowires. Review of Scientific Instruments 85 (1), 013901. https://doi.org/10.1063/1.4858815.

Chen, L.Y., *et al.*, 2015. Measuring surface dislocation nucleation in defect-scarce nanostructures. Nature Materials 14, 707–713. https://doi.org/10.1038/nmat4288.
Chen, Y., *et al.*, 2016. Effect of a high density of stacking faults on the young's modulus of GaAs nanowires. Nano Letters 16 (3), 1911–1916. https://doi.org/10.1021/acs.nanolett.5b05095.
Cheng, G., *et al.*, 2014. Mechanical properties of silicon carbide nanowires: Effect of size-dependent defect density. Nano Letters 14 (2), 754–758. https://doi.org/10.1021/nl404058r. (American Chemical Society).
Cheng, G., *et al.*, 2015. Large anelasticity and associated energy dissipation in single-crystalline nanowires. Nature Nanotechnology 10, 687–691.
Cheng, G., *et al.*, 2017. Anomalous tensile detwinning in twinned nanowires. Physical Review Letters 119 (25), 256101. https://doi.org/10.1103/PhysRevLett.119.256101.
Cheng, G., *et al.*, 2019. In situ nano-thermomechanical experiment reveals brittle to ductile transition in silicon nanowires. Nano Letters 19 (8), 5327–5334. https://doi.org/10.1021/acs.nanolett.9b01789.
Cheng, G., *et al.*, 2020. In-situ TEM study of dislocation interaction with twin boundary and retraction in twinned metallic nanowires. Acta Materialia 196, 304–312. https://doi.org/10.1016/j.actamat.2020.06.055.
Cuenot, S., *et al.*, 2004. Surface tension effect on the mechanical properties of nanomaterials measured by atomic force microscopy. Physical Review B 69. 165410.
Dai, S., *et al.*, 2015. Elastic properties of GaN Nanowires: Revealing the influence of planar defects on young's modulus at nanoscale. Nano Letters 15 (1), 8–15. https://doi.org/10.1021/nl501986d.
Desai, A.V., Haque, M.A., 2007. Mechanical properties of ZnO nanowires. Sensors and Actuators a-Physical 134 (1), 169–176.
Dikin, D.A., *et al.*, 2003. Resonance vibration of amorphous SiO_2 nanowires driven by mechanical or electrical field excitation. Journal of Applied Physics 93 (1), 226–230.
Ding, W., *et al.*, 2006. Mechanics of crystalline boron nanowires. Composites Science and Technology 66 (9), 1112–1124. https://doi.org/10.1016/j.compscitech.2005.11.030.
Espinosa, H.D., Zhu, Y., Moldovan, N., 2007. Design and operation of a MEMS-based material testing system for nanomechanical characterization. Journal of Microelectromechanical Systems 16 (5), 1219–1231.
Feng, X.L., *et al.*, 2007. Very high frequency silicon nanowire electromechanical resonators. Nano Letters 7 (7), 1953–1959.
Feng, X.L., *et al.*, 2010. Low voltage nanoelectromechanical switches based on silicon carbide nanowires. Nano Letters 10 (8), 2891–2896. https://doi.org/10.1021/nl1009734.
Filleter, T., *et al.*, 2012. Nucleation-controlled distributed plasticity in penta-twinned silver nanowires. Small 8 (19), 2986–2993. https://doi.org/10.1002/smll.201200522.
Ganesan, Y., *et al.*, 2010. Development and application of a novel microfabricated device for the in situ tensile testing of 1-D nanomaterials. Journal of Microelectromechanical Systems 19 (3), 675–682. https://doi.org/10.1109/JMEMS.2010.2046014.
Gianola, D.S., Eberl, C., 2009. Micro- and nanoscale tensile testing of materials. JOM 61, 24–35.
Gordon, M.J., *et al.*, 2009. Size effects in mechanical deformation and fracture of cantilevered silicon nanowires. Nano Letters 9 (2), 525–529. https://doi.org/10.1021/n1802556d.
Han, X., *et al.*, 2007. Low-temperature in situ large-strain plasticity of silicon nanowires. Advanced Materials 19, 2112–2118.
Han, X.D., *et al.*, 2005. Lattice bending, disordering, and amorphization induced plastic deformation in a SiC nanowire. Journal of Applied Physics 98 (12), https://doi.org/10.1063/1.2141654.
Haque, M.A., Espinosa, H.D., Lee, H.J., 2011. MEMS for in situ testing-handling, actuation, loading, and displacement measurements. MRS Bulletin 35 (05), 375–381. https://doi.org/10.1557/mrs2010.570.
He, M.-R., *et al.*, 2011. Quantifying the defect-dominated size effect of fracture strain in single crystalline ZnO nanowires. Journal of Applied Physics 109 (12), 123504. https://doi.org/10.1063/1.3594655.
He, R.R., *et al.*, 2008. Self-transducing silicon nanowire electromechanical systems at room temperature. Nano Letters 8 (6), 1756–1761.
Heidelberg, A., *et al.*, 2006. A generalized description of the elastic properties of nanowires. Nano Letters 6 (6), 1101–1106.
Hochbaum, A.I., *et al.*, 2008. Enhanced thermoelectric performance of rough silicon nanowires. Nature 451 (7175), 163. U5.
Hoffmann, S., *et al.*, 2006. Measurement of the bending strength of vapor-liquid-solid grown silicon nanowires. Nano Letters 6 (4), 622–625.
Hoffmann, S., *et al.*, 2007. Fracture strength and Young's modulus of ZnO nanowires. Nanotechnology 18 (20), 205503.
Hosseinian, E., Pierron, O.N., 2013. Quantitative in situ TEM tensile fatigue testing on nanocrystalline metallic ultrathin films. Nanoscale 5 (24), 12532–12541. https://doi.org/10.1039/c3nr04035f.
Huang, J.Y., *et al.*, 2010. In situ observation of the electrochemical lithiation of a single SnO_2 nanowire electrode. Science 330 (6010), 1515–1520. https://doi.org/10.1126/science.1195628. (American Association for the Advancement of Science).
Hwang, B., *et al.*, 2015. Effect of surface energy on size-dependent deformation twinning of defect-free Au nanowires. Nanoscale 7 (38), 15657–15664. https://doi.org/10.1039/c5nr03902a. (Royal Society of Chemistry).
Javey, A., *et al.*, 2007. Layer-by-layer assembly of nanowires for three-dimensional, multifunctional electronics. Nano Letters 7 (3), 773–777.
Jing, G.Y., *et al.*, 2006. Surface effects on elastic properties of silver nanowires: Contact atomic-force microscopy. Physical Review B 73. 235409.
Johansson, S., *et al.*, 1988. Fracture testing of silicon microelements in situ in a scanning electron microscope. Journal of Applied Physics 63 (10), 4799–4803. https://doi.org/10.1063/1.340471.
Kang, W., Saif, M.T.A., 2013. In situ study of size and temperature dependent brittle-to-ductile transition in single crystal silicon. Advanced Functional Materials 23 (6), 713–719.
Kim, C., *et al.*, 2008. Copper nanowires with a five-twinned structure grown by chemical vapor deposition. Advanced Materials 20 (10), 1859–1863. https://doi.org/10.1002/adma.200701460.
Kim, Y.-J., *et al.*, 2011. Exploring nanomechanical behavior of silicon nanowires: AFM bending versus nanoindentation. Advanced Functional Materials 21 (2), 279–286. https://doi.org/10.1002/adfm.201001471. (WILEY-VCH Verlag).
Law, M., *et al.*, 2005. Nanowire dye-sensitized solar cells. Nature Materials 4 (6), 455–459.
Lee, P., *et al.*, 2012. Highly stretchable and highly conductive metal electrode by very long metal nanowire percolation network. Advanced Materials 24 (25), 3326–3332. https://doi.org/10.1002/adma.201200359.
Lee, S., *et al.*, 2014. Reversible cyclic deformation mechanism of gold nanowires by twinning-detwinning transition evidenced from in situ TEM. Nature Communications 5, 3033. https://doi.org/10.1038/ncomms4033.
Li, C., Cheng, G., *et al.*, 2020. Microelectromechanical systems for nanomechanical testing: Displacement- and force-controlled tensile testing with feedback control. Experimental Mechanics 60 (7), 1005–1015. https://doi.org/10.1007/s11340-020-00619-z. (Springer).
Li, C., Zhang, D., *et al.*, 2020. Microelectromechanical systems for nanomechanical testing: Electrostatic actuation and capacitive sensing for high-strain-rate testing. Experimental Mechanics 60 (3), 329–343. https://doi.org/10.1007/S11340-019-00565-5/FIGURES/15. (Springer).
Li, Q., *et al.*, 2007. Silicon nanowire electromechanical switches for logic device application. Nanotechnology 18 (31), 315202. https://doi.org/10.1088/0957-4484/18/31/315202.
Li, X.D., Chasiotis, I., Kitamura, T., 2010. In situ scanning probe microscopy nanomechanical testing. MRS Bulletin 35 (5), 361–367.
Li, X.X., *et al.*, 2003. Ultrathin single-crystalline-silicon cantilever resonators: Fabrication technology and significant specimen size effect on Young's modulus. Applied Physics Letters 83 (15), 3081–3083.
Liang, H.Y., Upmanyu, M., Huang, H.C., 2005. Size-dependent elasticity of nanowires: Nonlinear effects. Physical Review B 71 (24), 241403.
Liu, B., *et al.*, 2005. Needlelike bicrystalline GaN nanowires with excellent field emission properties. Journal of Physical Chemistry B 109 (36), 17082–17085. https://doi.org/10.1021/jp052827r.
Liu, Z., *et al.*, 2003. Synthesis of copper nanowires via complex-surfactant-assisted hydrothermal reduction process. Journal of Physical Chemistry B 107, 12658–12661.

Lu, Y., *et al.*, 2011. Surface dislocation nucleation mediated deformation and ultrahigh strength in sub-10-nm gold nanowires. Nano Research 4 (12), 1261–1267. https://doi.org/10.1007/s12274-011-0177-y.

McAlpine, M.C., *et al.*, 2003. High-performance nanowire electronics and photonics on glass and plastic substrates. Nano Letters 3 (11), 1531–1535.

McAlpine, M.C., *et al.*, 2007. Highly ordered nanowire arrays on plastic substrates for ultrasensitive flexible chemical sensors. Nature Materials 6 (5), 379–384.

Murphy, C.J., Jana, N.R., 2002. Controlling the aspect ratio of inorganic nanorods and nanowires. Acta Materialia 14 (1), 80–82.

Murphy, K.F., *et al.*, 2014. Strain- and defect-mediated thermal conductivity in silicon nanowires. Nano Letters 14 (7), 3785–3792. https://doi.org/10.1021/nl500840d. (American Chemical Society).

Murphy, K.F., Chen, L.Y., Gianola, D.S., 2013. Effect of organometallic clamp properties on the apparent diversity of tensile response of nanowires. Nanotechnology 24 (23), 235704. https://doi.org/10.1088/0957-4484/24/23/235704.

Nakao, S., *et al.*, 2006. Mechanical properties of a micron-sized SCS film in a high-temperature environment. Journal of Micromechanics and Microengineering 16 (4), 715–720.

Nam, C.Y., *et al.*, 2006. Diameter-dependent electromechanical properties of GaN nanowires. Nano Letters 6 (2), 153–158.

Narayanan, S., *et al.*, 2015. Strain hardening and size effect in five-fold twinned Ag nanowires. Nano Letters 15 (6), 4037–4044.

Ngo, L.T., *et al.*, 2006. Ultimate-strength germanium nanowires. Nano Letters 6 (12), 2964–2968. https://doi.org/10.1021/nl0619397.

Ni, H., Li, X.D., 2006. Young's modulus of ZnO nanobelts measured using atomic force microscopy and nanoindentation techniques. Nanotechnology 17 (14), 3591–3597.

Ni, H., Li, X.D., Gao, H.S., 2006. Elastic modulus of amorphous SiO_2 nanowires. Applied Physics Letters 88, 4.

Park, H.S., *et al.*, 2009. Mechanics of crystalline nanowires. MRS Bulletin 34 (03), 178–183.

Park, H.S., Zimmerman, J.A., 2005. Modeling inelasticity and failure in gold nanowires. Physical Review B 72. 54106.

Paulo, A.S., *et al.*, 2005. Mechanical elasticity of single and double clamped silicon nanobeams fabricated by the vapor-liquid-solid method. Applied Physics Letters 87. 53111.

Pearson, G., Read, W., Feldmann, W., 1957. Deformation and fracture of small silicon crystals. Acta Metallurgica 5 (4), 181–191. https://doi.org/10.1016/0001-6160(57)90164-5.

Peng, C., *et al.*, 2012. Size dependent mechanical properties of single crystalline nickel nanowires. Journal of Applied Physics 111 (6), https://doi.org/10.1063/1.3698625.

Peng, C., *et al.*, 2013. Strain rate dependent mechanical properties in single crystal nickel nanowires. Applied Physics Letters 102 (8), https://doi.org/10.1063/1.4793481.

Petrova, H., *et al.*, 2006. Crystal structure dependence of the elastic constants of gold nanorods. Journal of Materials Chemistry 16 (40), 3957–3963.

Poncharal, P., *et al.*, 1999. Electrostatic deflections and electromechanical resonances of carbon nanotubes. Science 283 (5407), 1513–1516.

Qin, Q., *et al.*, 2012. Measuring true young's modulus of a cantilevered nanowire: Effect of clamping on resonance frequency. Small 8 (16), 2571–2576.

Qin, Q., *et al.*, 2015. Recoverable plasticity in penta-twinned metallic nanowires governed by dislocation nucleation and retraction. Nature Communications 6, 5983. https://doi.org/10.1038/ncomms6983. (Nature Publishing Group).

Ramachandramoorthy, R., *et al.*, 2016. High strain rate tensile testing of silver nanowires: Rate-dependent brittle-to-ductile transition. Nano Letters 16 (1), 255–263. https://doi.org/10.1021/acs.nanolett.5b03630. (American Chemical Society).

Ramachandramoorthy, R., Bernal, R., Espinosa, H.D., 2015. Pushing the envelope of in situ transmission electron microscopy. ACS Nano 9 (5), 4675–4685. https://doi.org/10.1021/acsnano.5b01391. (American Chemical Society).

Richter, G., *et al.*, 2009. Ultra high strength single crystalline nanowhiskers grown by physical vapor deposition. Nano Letters 9, 3048–3052.

Salvetat, J.P., *et al.*, 1999. Elastic and shear moduli of single-walled carbon nanotube ropes. Physical Review Letters 82 (5), 944–947. Available at: isi:000078412900019.

Sedlmayr, A., *et al.*, 2012. Existence of two twinning-mediated plastic deformation modes in Au nanowhiskers. Acta Materialia 60 (9), 3985–3993. https://doi.org/10.1016/j.actamat.2012.03.018.

Seo, J.H., *et al.*, 2013. Origin of size dependency in coherent-twin-propagation-mediated tensile deformation of noble metal nanowires. Nano Letters 13 (11), 5112–5116. https://doi.org/10.1021/nl402282n.

Seo, J.-H., *et al.*, 2011. Superplastic deformation of defect-free Au nanowires via coherent twin propagation. Nano Letters 11 (8), 3499–3502. https://doi.org/10.1021/nl2022306. (American Chemical Society).

Shim, H.W., *et al.*, 2005. Nanoplate elasticity under surface reconstruction. Applied Physics Letters 86. 151912.

Song, J.H., *et al.*, 2005a. Elastic property of vertically aligned nanowires. Nano Letters 5 (10), 1954–1958.

Song, J.H., *et al.*, 2005b. Elastic property of vertically aligned nanowires. Nano Letters 5 (10), 1954–1958.

Steighner, M.S., 2011. Dependence on diameter and growth direction of apparent strain to failure of Si nanowires. Journal of Applied Physics 109 (3).

Sun, Y., *et al.*, 2002. Crystalline silver nanowires by soft solution processing. Nano Letters 2 (2), 165–168. https://doi.org/10.1021/nl010093y. (American Chemical Society).

Tabib-Azar, M., *et al.*, 2005. Mechanical properties of self-welded silicon nanobridges. Applied Physics Letters 87. 113102.

Takei, K., *et al.*, 2010. Nanowire active-matrix circuitry for low-voltage macroscale artificial skin. Nature Materials 9 (10), 821–826. https://doi.org/10.1038/nmat2835. (Nature Publishing Group).

Tang, D.-M., *et al.*, 2012. Mechanical properties of Si nanowires as revealed by in situ transmission electron microscopy and molecular dynamics simulations. Nano Letters 12 (4), 1898–1904. https://doi.org/10.1021/nl204282y. (American Chemical Society).

Tian, M., *et al.*, 2003. Electrochemical growth of single-crystal metal nanowires via a two-dimensional nucleation and growth mechanism. Nano Letters 3 (7), 919–923. https://doi.org/10.1021/nl034217d. (American Chemical Society).

Treacy, M.M.J., Ebbesen, T.W., Gibson, J.M., 1996. Exceptionally high Young's modulus observed for individual carbon nanotubes. Nature 381 (6584), 678–680. Available at: isi:A1996UR97900045.

Tsuchiya, T., *et al.*, 2012. Electrostatic tensile testing device with nanonewton and nanometer resolution and its application to nanowire testing. Journal of Microelectromechanical Systems 21, 523–529.

Tsuchiya, T., *et al.*, 2018. Tensile strength of silicon nanowires batch-fabricated into electrostatic MEMS testing device. Applied Sciences 8 (6), https://doi.org/10.3390/app8060880.

Wagner, A., *et al.*, 2015. Mechanisms of plasticity in near-theoretical strength sub-100 nm Si nanocubes. Acta Materialia 100, 256–265.

Wang, J., *et al.*, 2013. Near-ideal theoretical strength in gold nanowires containing angstrom scale twins. Nature Communications 4, 1742. https://doi.org/10.1038/ncomms2768. (Nature Publishing Group, a division of Macmillan Publishers Limited. All Rights Reserved).

Wang, Y.B., *et al.*, 2011. Super deformability and young's modulus of gaas nanowires. Advanced Materials 23 (11), 1356–1360. https://doi.org/10.1002/adma.201004122.

Wang, Z.L., 2003. Nanowires and Nanobelts, Materials, Properties and Devices. I. Kluwer Academic Publishers.

Wang, Z.L., Song, J.H., 2006. Piezoelectric nanogenerators based on zinc oxide nanowire arrays. Science 312 (5771), 242–246.

Weinberger, C.R., Cai, W., 2012. Plasticity of metal nanowires. Journal of Materials Chemistry 22 (8), 3277–3292. https://doi.org/10.1039/c2jm13682a. (The Royal Society of Chemistry).

Wen, B., Sader, J.E., Boland, J.J., 2008. Mechanical properties of ZnO nanowires. Physical Review Letters 101. 175502.

Wiley, B., *et al.*, 2005. Shape-controlled synthesis of metal nanostructures: The case of silver. Chemistry-A European Journal 11 (2), 454–463.

Wiley, B., Sun, Y., Xia, Y., 2007. Synthesis of silver nanostructures with controlled shapes and properties. Accounts of Chemical Research 40 (10), 1067–1076. https://doi.org/10.1021/ar7000974. (American Chemical Society).

Wong, E.W., Sheehan, P.E., Lieber, C.M., 1997. Nanobeam mechanics: Elasticity, strength, and toughness of nanorods and nanotubes. Science 277, 1971–1975.

Wu, B., *et al.*, 2006. Microstructure-hardened silver nanowires. Nano Letters 6 (3), 468–472.

Wu, B., Heidelberg, A., Boland, J.J., 2005. Mechanical properties of ultrahigh-strength gold nanowires. Nature Materials 4 (7), 525–529. Available at: isi:000230190900014.

Xia, Y., *et al.*, 2003. One-dimensional nanostructures: Synthesis, characterization, and applications. Advanced Materials 15 (5), 353–389.

Xu, F., *et al.*, 2010. Mechanical properties of ZnO nanowires under different loading modes. Nano Research 3, 271–280.
Xu, F., Zhu, Y., 2012. Highly conductive and stretchable silver nanowire conductors. Advanced Materials 24 (37), 5117–5122.
Xu, F., Lu, W., Zhu, Y., 2011. Controlled 3D buckling of silicon nanowires for stretchable electronics. Acs Nano 5 (1), 672–678.
Yang, W., *et al.*, 2005. Single-crystal SiC nanowires with a thin carbon coating for stronger and tougher ceramic composites. Advanced Materials 17 (12), 1519–1523. https://doi.org/10.1002/adma.200500104. (WILEY-VCH Verlag).
Yao, S., *et al.*, 2017. Soft electrothermal actuators using silver nanowire heaters. Nanoscale 9 (11), 3797–3805. https://doi.org/10.1039/C6NR09270E. (Royal Society of Chemistry).
Yao, S., *et al.*, 2019. Nanomaterial-enabled flexible and stretchable sensing systems: Processing, integration, and applications. Advanced Materials 32. 1902343. https://doi.org/10.1002/adma.201902343.
Yao, S., Zhu, Y., 2014. Wearable multifunctional sensors using printed stretchable conductors made of silver nanowires. Nanoscale 6 (4), 2345–2352. https://doi.org/10.1039/c3nr05496a. (The Royal Society of Chemistry).
Yao, S., Zhu, Y., 2015. Nanomaterial-enabled stretchable conductors: Strategies, materials and devices. Advanced Materials 27 (9), 1480–1511. https://doi.org/10.1002/adma.201404446.
Yao, S., Swetha, P., Zhu, Y., 2018. Nanomaterial-enabled wearable sensors for healthcare. Advanced Healthcare Materials 7 (1), 1700889. (Wiley-Blackwell). https://doi.org/10.1002/adhm.201700889.
Yilmaz, M., Kysar, J.W., 2013. Monolithic integration of nanoscale tensile specimens and MEMS structures. Nanotechnology 24. 165502.
Yin, S., Cheng, G., Richter, G., *et al.*, 2019. Transition of deformation mechanisms in single-crystalline metallic nanowires. ACS Nano 13 (8), 9082–9090. https://doi.org/10.1021/acsnano.9b03311.
Yin, S., Cheng, G., Chang, T.H., *et al.*, 2019. Hydrogen embrittlement in metallic nanowires. Nature Communications 10 (1), 2004. https://doi.org/10.1038/s41467-019-10035-0. (Nature Publishing Group).
Yoo, Y., *et al.*, 2010. Steering epitaxial alignment of Au, Pd, and AuPd nanowire arrays by atom flux change. Nano Letters 10 (2), 432–438. https://doi.org/10.1021/nl903002x. (American Chemical Society).
Yu, M.F., *et al.*, 2000. Strength and breaking mechanism of multiwalled carbon nanotubes under tensile load. Science 287 (5453), 637–640.
Zhang, D., *et al.*, 2010. In situ electron microscopy mechanical testing of silicon nanowires using electrostatically actuated tensile stages. Journal of Microelectromechanical Systems 19 (3), 663–674. https://doi.org/10.1109/JMEMS.2010.2044746.
Zhang, D.F., *et al.*, 2009. A high-sensitivity and quasi-linear capacitive sensor for nanomechanical testing applications. Journal of Micromechanics and Microengineering 19 (7), 075003.
Zhang, H., *et al.*, 2008. Atomic force microscopy measurement of the Young's modulus and hardness of single LaB[sub 6] nanowires. Applied Physics Letters 92 (17), 173121. https://doi.org/10.1063/1.2919718.
Zhang, H., *et al.*, 2016. Approaching the ideal elastic strain limit in silicon nanowires. Science Advances 2 (8), e1501382.
Zhang, Y., *et al.*, 2011. Piezoresistivity characterization of synthetic silicon nanowires using a MEMS device. Journal of Microelectromechanical Systems 20 (4), 959–967.
Zhou, L.G., Huang, H.C., 2004. Are surfaces elastically softer or stiffer? Applied Physics Letters 84 (11), 1940–1942.
Zhou, W., *et al.*, 2020. Gas-permeable, ultrathin, stretchable epidermal electronics with porous electrodes. ACS Nano 14 (5), 5798–5805. https://doi.org/10.1021/acsnano.0c00906. (American Chemical Society).
Zhu, T., Li, J., 2010. Ultra-strength materials. Progress in Materials Science 55 (7), 710–757.
Zhu, Y., *et al.*, 2009. Mechanical properties of vapor-liquid-solid synthesized silicon nanowires. Nano Letters 9, 3934–3939.
Zhu, Y., *et al.*, 2012. Size effects on elasticity, yielding and fracture of silver nanowires: In situ experiments. Physical Review B 85. 45443.
Zhu, Y., 2016. In situ nanomechanical testing of crystalline nanowires in electron microscopes. JOM 68, 84–93. https://doi.org/10.1007/s11837-015-1614-2.
Zhu, Y., 2017. Mechanics of crystalline nanowires: An experimental perspective. Applied Mechanics Reviews 69 (1), 010802. https://doi.org/10.1115/1.4035511.
Zhu, Y., Espinosa, H.D., 2005. An electromechanical material testing system for in situ electron microscopy and applications. Proceedings of the National Academy of Sciences of the United States of America 102 (41), 14503–14508.
Zhu, Y., Chang, T.-H., 2015. A review of microelectromechanical systems for nanoscale mechanical characterization. Journal of Micromechanics and Microengineering 25 (9), 093001. https://doi.org/10.1088/0960-1317/25/9/093001.
Zhu, Y., Moldovan, N., Espinosa, H.D., 2005. A microelectromechanical load sensor for in situ electron and x-ray microscopy tensile testing of nanostructures. Applied Physics Letters 86. 13506.
Zhu, Y., Corigliano, A., Espinosa, H.D., 2006. A thermal actuator for nanoscale in situ microscopy testing: Design and characterization. Journal of Micromechanics and Microengineering 16 (2), 242–253.
Zhu, Y., Ke, C., Espinosa, H.D., 2007. Experimental techniques for the mechanical characterization of one-dimensional nanostructures. Experimental Mechanics 47 (1), 7–24.